



Università di Pisa

---

DIPARTIMENTO DI FISICA "ENRICO FERMI"

Corso di Laurea in Fisica

TESI DI LAUREA

## Commissioning and first data analysis of the Mainz radius experiment.

Candidato:

**Adriano Del Vincio**

Matricola 562946

Relatore:

**Prof. Francesco Forti**

**Prof.ssa Concettina Sfienti**

# Contents

<b>1 Physics motivation for neutron skin thickness measurement.</b>	<b>2</b>
1.1 Nuclear equation of state (EOS) and neutron skin thickness.	2
1.2 Parity-violating scattering experiment	2
1.3 Transverse asymmetry	2
1.3.1 Motivation	2
1.3.2 Conventions used	3
<b>2 Transverse Asymmetry</b>	<b>4</b>
2.1 Description of the process	4
2.1.1 Elastic scattering	5
2.1.2 Inelastic scattering	5
2.1.3 Model description	6
2.2 State of the Experiment	6
<b>3 Experimental setup.</b>	<b>8</b>
3.1 Overview of the experiment	8
3.2 Mami	10
3.2.1 Acceleration stage	10
3.2.2 Polarized Beam	10
3.2.3 Polarization measurement	11
3.3 Experimental hall setup	12
3.4 Detectors and beam monitors	12
3.4.1 Detectors A and B	12
3.4.2 Beam monitors	14
3.4.3 Beam stabilization	16
3.5 Electronics	16
3.5.1 VFCs	16
3.5.2 Nino board	17
3.5.3 Master Board	17
<b>4 Detectors Test, alignment and calibrations.</b>	<b>18</b>
4.1 Data tree	18
4.2 Detectors test	18
4.3 Calibrations	23
4.3.1 Alignment of the scattering plane	23
4.3.2 Calibration of the VFCs monitors	23
4.3.3 Calibration of the PIMO monitors	23
4.3.4 Current (PIMO) and energy monitors (ENMO) calibration	25
4.3.5 Calibration of the pmts	26
4.3.6 Autocalibration procedure	30
<b>5 Data Analysis: Asymmetry on Carbon and Rates on Lead target.</b>	<b>33</b>
5.1 Rates on lead	33
5.2 Model for fitting the data	33
5.3 Data pre-selection and Fit	34
5.4 False asymmetries	39
5.5 ??Bootstrap??	42
<b>6 Result</b>	<b>43</b>

7 Conclusion and outlook	45
Appendices	46
A Some Appendix	47

### **Abstract**

**Short introduction (2-3 pages) to the thesis, it's an entire overview of the entire thesis, and a reader should have a clear opinion of what is inside the thesis.**

# Chapter 1

## Physics motivation for neutron skin thickness measurement.

- explain neutron skin thickness.
- connection to neutron stars radius, and neutron stars description.
- Equation of state (EoS) for high density nuclear matter.
- Parity-violating scattering experiment for extracting neutron skin thickness.
- mention the weak form factor.
- Transverse asymmetry as background for Parity-violating experiment.
- Mention the other experiment, like PREX, that measure zero  $A_n$  for Lead.

### 1.1 Nuclear equation of state (EOS) and neutron skin thickness.

In this section we have to explain what is the neutron skin thickness and why this parameter is related to the Equation of State for nuclear matter (in particular, the slope of the Symmetry energy in the semiempirical mass formula). Then, explain the parallelism between Neutron stars and Nuclear matter (they share the same EOS), and underline the relation between radius of the neutron stars and EOS.

### 1.2 Parity-violating scattering experiment

This section is for describing the way it's possible to extract the neutron skin thickness. Here I have to mention the weak form factor and the important fact that the neutrons are more important than the protons in the parity-violating scattering, because of the weak mixing angle.

### 1.3 Transverse asymmetry

Here we have to introduce the aim of this thesis: the transverse asymmetry is a source of background for the parity-violating experiments. Furthermore the theory is not working well for some nuclei ( $^{208}Pb$ ), so mention PREX paper about the last measurement on carbon and lead, the problem that they measure 0 transverse asymmetry.

#### 1.3.1 Motivation

Here present all the motivation for this thesis, so the fact that we want to measure the rates on lead for the future experiment, test the new electronics, measure another time the transverse asymmetry on  $^{12}C$ .

### 1.3.2 Conventions used

It could be usefull, here, to have a subsection to explain the terminology for this thesis, to avoid misunderstanding.

# Chapter 2

## Transverse Asymmetry

- Physics behind the  $A_n$  asymmetry, dependence on  $Q^2$ , the formula  $\frac{\sigma_{\uparrow} - \sigma_{\downarrow}}{\sigma_{\uparrow} + \sigma_{\downarrow}}$
- state of the art of the Exp.
- Model description: so scattering amplitude, theoretical prediction
- Expected error  $\delta A_t$
- open question: problems with lead, dependence of  $E_{beam}$ , dependence from Z, Z/A

### 2.1 Description of the process

Explain the scattering process we are studying (at least one figure to visualize the kinematics of the scattering). Mention the link between this process and time-reversal operator. Add two figures for elastic and inelastic scattering.

The Beam Normal single spin asymmetry, which we will refer for brevity as Transverse asymmetry, originates from the interference of two scattering process. For the purpose of this thesis, we will present the case of electron scattering against a spin 0 target [4]. To understand why the interference of this two scattering amplitude give rise to an asymmetry, we first have to look at the kinematic of the experiment:

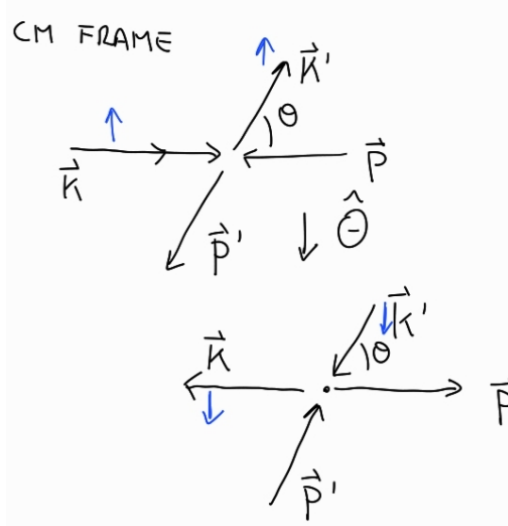


Figure 2.1: •

Where all the momenta are measured respect to the center of mass frame. In the figure we can confront the two situation before and after applying the Time-reversal operator,  $\hat{\Theta}$ . Looking at the picture we can understand that :

- Before applying  $\hat{\Theta}$ , we have the incident electron with  $\vec{k}$  momenta and the nucleus with  $\vec{P}$  momenta, after applying  $\hat{\Theta}$  we have that the incident/outgoing electron and the incident/outgoing nucleus are exchanged.

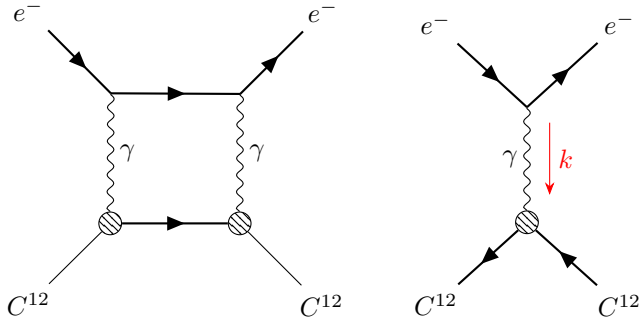


Figure 2.2: TPE and OPE diagrams in electron nucleus scattering.

- The  $\hat{\Theta}$  operator acts also on the spin of the electron. Because we are considering process where the spin doesn't flip, the two situations are not equivalent.
- Considering that the process is elastic, the kinematic is the same, taking  $\vec{p}$  and  $\vec{k}$  as the initial particle momenta, or  $\vec{p}'$  and  $\vec{k}'$ .

The time-reversal operator seems to connect the two different cases of UP and DOWN polarized electron. Our effort is to measure the asymmetry between the two cross section:

$$A = \frac{\sigma_{\uparrow} - \sigma_{\downarrow}}{\sigma_{\uparrow} + \sigma_{\downarrow}} \quad (2.1)$$

And it's particularly clear that a non-zero asymmetry depends on how the time-reversal act on the elastic amplitude of the process.

With this idea, let's see in more detail the  $\hat{\Theta}$ . We know that  $\hat{\Theta}$  is an antiunitary operator that can be always seen as:

$$\hat{\Theta} = U \cdot K$$

Where  $U$  is an unitary operator, while  $K$  is the complex conjugation operator that generates the complex conjugate of each coefficient in front of it. If we consider a ket describing a system we have that:

$$Kc|\alpha\rangle = c^*K|\alpha\rangle \quad (2.2)$$

Now, let's consider  $H$  as the hamiltonian of our system. We want to apply the  $\hat{\Theta}$  operator. We can now use the assumption that the hamiltonian consist of two term, which correspond to the two different scattering process. Because of the electromagnetic interaction conserve  $CP$ , so also  $T$  is conserved, we know in advance that each piece of the hamiltonian commute with  $\hat{\Theta}$ . Now let's see what happen for an hamiltonian which has an imaginary part:

$$H = H_R + iH_{Im} \quad ; \quad \hat{\Theta}H\hat{\Theta}^{-1} = \hat{\Theta}H_R\hat{\Theta}^{-1} + \hat{\Theta}iH_{Im}\hat{\Theta}^{-1} \Rightarrow H_R - iH_{Im} \neq H \quad (2.3)$$

what we understand from these simple calculation is that to give rise to an asymmetry, we expect an imaginary part of the scattering amplitude different from zero.

At the  $\alpha$  leading order, the two process of the electron-Nucleus scattering that give rise to the asymmetry involve the exchange of one-photon-exchange (OPE) and two-photon-exchange (TPE). The Feynman diagrams that describes the processes are the following:

A seguire come si scrive l'ampiezza per il termine elastico ed inelastico, aggiungere in appendice come viene fatto l'integrale sullo spazio delle fasi e stop.

### 2.1.1 Elastic scattering

Write the amplitude for the elastic (how to manipulate expression, maybe in the appendix).

### 2.1.2 Inelastic scattering

Explain how it's possible to compute the inelastic expression, what kind of approximations are used (optical theorem...)

### 2.1.3 Model description

Present the theoretical formula for the Transverse asymmetry, and comment on energy, Z, Z/A dependencies adding together the elastic and inelastic contributions, we end with the following formula which describes the process [3]:

$$A_N = C_0 \cdot \log\left(\frac{Q^2}{m_e^2 c^2}\right) \frac{F_{Compton}(Q^2)}{F_{ch}(Q^2)} \quad (2.4)$$

## 2.2 State of the Experiment

Write down the formula  $\frac{\sigma_{\uparrow} - \sigma_{\downarrow}}{\sigma_{\uparrow} + \sigma_{\downarrow}}$ . Hints at how to measure the Transverse asymmetry (remember to mention we have a polarized beam against a unpolarized target). Explain the expected error for the reconstructed asymmetry. Furthemore talk about the last mesurements obtained by the other collaborations, an outlook of the current situation. Maybe add also how we proceed to measure the transverse asymmetry, so the structure of the event, polarities patterns...

We have seen so far how the Transverse Asymmetry is related to the interference between two scattering amplitude, and the theoretical model used to describe the process. The goal from an experimental point of view is to measure this quantity. The challenge is to obtain a valid measure of  $A_n$ , which is of the order of 20 part per million (ppm), taking into consideration all the possible effects that can interfere. To measure  $A_n$ , the straighforward method is to prepare an electron beam, with polarized electron, and send it to a fixed target. The scattered electrons are then collected by a detector placed at a certain angle, and now it's possible to obtain the trasverse asymmetry applying the formula:

$$A(Q, p) = \frac{N_{\uparrow}(Q) - N_{\downarrow}(Q)}{N_{\uparrow}(Q) + N_{\downarrow}(Q)} \cdot \left(\frac{1}{p}\right) \quad (2.5)$$

where we have explained the dependence on the transmitted impulse, on the degree of polarization of the beam. In an experiment of this type, several requests are necessary to have an effective data acquisition:

- The accelerator must produce a polarized beam, stable over the time, with an high polarization percentage, in order to amplify the effect.
- The Beam energy needs to be quite stable, and should not depend on the Polarization state of the electrons. A change in the Beam energy associated with the polarization state, can lead to a different count rate for  $N_{\uparrow}$  and  $N_{\downarrow}$ , would make a contribution that would be added to that of the physical process
- The beam must be correctly aligned with the target, and stable. Again if the position of the target changes accordin to the polarization of the electrons, it will produce another contribution to the total asymmetry.
- The beam current should not depend on the polarization state of the electrons. If the beam source depends on the polarization, we will have a difference in the event rate and then another false asymmetry.
- it's necessary to reject possible double elastic scattering events, which may contribute to the total asymmetry.

All this demands can be satisfied with an accelerator that has stabilization devices with great precision and that can sustain high beam intensities. This last request is necessary to accumulate enough statistics to measure the transvere asymmetry with an accuracy about 1 ppm, in view of the future PV experiments. We can quantify how the statistical error varies according to the amount of data avaible. With the quite general assumption that the measured rate  $N_{\uparrow, \downarrow}$  are gaussian distributed variables, we can compute the expected variance of  $A_n$ :

$$Var[A_n] = \frac{1 - A^2}{N_{\uparrow} + N_{\downarrow}} \quad (2.6)$$

This is the variance associated to a single measurement of the transverse asymmetry. As is well known, the variance scales as  $\frac{1}{n}$  as  $n$ , the number of measures, increases. Beacause the  $A_n$  is expected to be quite small, we can approximate the above formula:

$$V[A_n] = \frac{1}{2N \cdot n} \quad (2.7)$$

The error associated to the reconstructed asymmetry is the square root of the above quantity. If we impose that the error must be  $\leq 1ppm$  we can easily obtain that the quantity  $n \cdot N$ :

$$n \cdot N \leq \frac{1}{2} \cdot 10^{12}$$

We will see later that achievable rates  $N_{\uparrow,\downarrow}$  are in the range (20000,100000) for a carbon target. This number can not be increased at will by acting on the beam current. The first reason is obvious: the accelerator and the beam source can handle only a certain amount of electrons before losing their characteristics, furthermore a beam with great intensity for an extended periods of time can damage the carbon target, up to the risk of melting it. Another idea might be to increase the thickness of the target, to take advantage of the larger cross section. However this does not take into account that by doing so the number of double scattering event is increased. To avoid this the scientific community that deals with these nuclear physics measurements respect the convention that the target thickness should be less than the 10% of the radiation length of the material.

# Chapter 3

## Experimental setup.

- description of MAMI, how the beam is produced, how the electrons are polarized.
- description of A1.
- description of beam stabilization, how the monitors measure the beam parameters.
- Electronics description, DAQ system, VFC monitors.
- Detectors A and B.

### 3.1 Overview of the experiment.

To measure the Beam-Normal single spin asymmetry, a polarized beam of 570 MeV will be sent against a 10 mm  $^{12}\text{C}$  target. The detectors consist of two fused-silica coupled to 3 (detector B) and 8 (detector A) pmts, which collect the Cherenkov light emitted when an electron pass through the fused-silica. The detector are placed inside the two spectrometer of the A1 hall, which are not used in this experiment due to the high luminosity of the beam ( $20 \mu\text{A}$ ) that is away from their good point of operation. The photomultipliers asymmetry due the change of the electrons spin is the target of the measurement. The pmts signals are collected and digitalized by the **NINO** board, after a threshold selection, and sent to the A1 control room computer, where the DAQ program collect the data together with all the data coming from the Beam monitors producing Binary files, which are later analyzed by the analysis program, which is significant part of the work done in the framework of the thesis. The data collected are divided in *Events* made by 4 *sub-events* in sequence. Each event correspond to a temporal window of  $\simeq 80 \mu\text{s}$ , where each sub-event is  $20 \mu\text{s}$  long. Here it's important to clarify that unlike the majority of experiments in high energy physics, an event is made by all the electrons interacting with the detectors during the time interval of the event, and we will refer to this hereafter unless otherwise stated. The division into sub-events reflects the polarization sequence of the beam. The PMTS counts and the beam monitor values are saved for each subevent, along with the time lenght of the event (measured by in clock cycle by the NINO electronic board 3.5.2), and other values which are required to process beam monitor data.

The general structure of the event is the following:

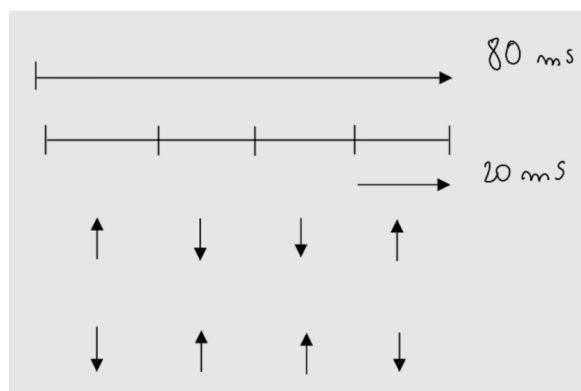


Figure 3.1: Event structure

The two polarity pattern are selected randomly using a De Bruijng sequence, (**spiegare cosa è e come è implementata**). For each event the asymmetry  $A_n$  is computed, along with

## 3.2 Mami

How Mami produces polarized electron and how the particle are accelerated (the way Mainz Mikroton is working is completely different from the other accelerators, so maybe this section will be too long).

### 3.2.1 Acceleration stage.

explain how electrons are accelerated, and sent to different experiments.

### 3.2.2 Polarized Beam.

Here a subsection to explain how the polarized electrons are produced. Important to mention the systematic error for the polarization mesurement (in our beam time we couldn't measure with Moller polarimeter, so this discussion is important for future experiment, however it's important to say something about it). Remember to explain how the spin are rotated to the transverse plane, and the  $\frac{\lambda}{2}$

For the beam-normal single spin asymmetry a vertical polarized beam is necessary. At the MAMI electron accelerator is possible to produce a vertical polarized beam with energy in the range 180 MeV – 855 MeV [5]. In this section the procedure to orient the beam vertically is presented, following an explanation of how the degree of polarization of the beam is measured.

The electron source used at MAMI is made by a strained GaAs/GaAsP superlattice photocathode illuminated by circular polarized light. A Pockels cell changes the helicity of the photons impinging on the electrons. The extracted electron has the same helicity of the incoming photon, let's suppose as an example:

$$(Jz)_\gamma = \pm 1 \quad (Jz)_{e^-} = \mp \frac{1}{2} \rightarrow \pm \frac{1}{2} \quad (3.1)$$

With the fast change of the Pockels cell it is possible to alternately revert the sign of the polarization. By the insertion of a  $\lambda/2$  plate between the laser system and the photocathode the polarization orientation of the electron beam can be reversed for each sub-event, useful later for the estimation of systematic errors. The beam polarization achieved with this source is roughly 80%, for the beam time it was : 0.79%

To switch from longitudinal polarization to transverse polarisation, two devices are used: the **Wien filter** and a **double solenoid** located in the injection beam line.

*bird's eye view*

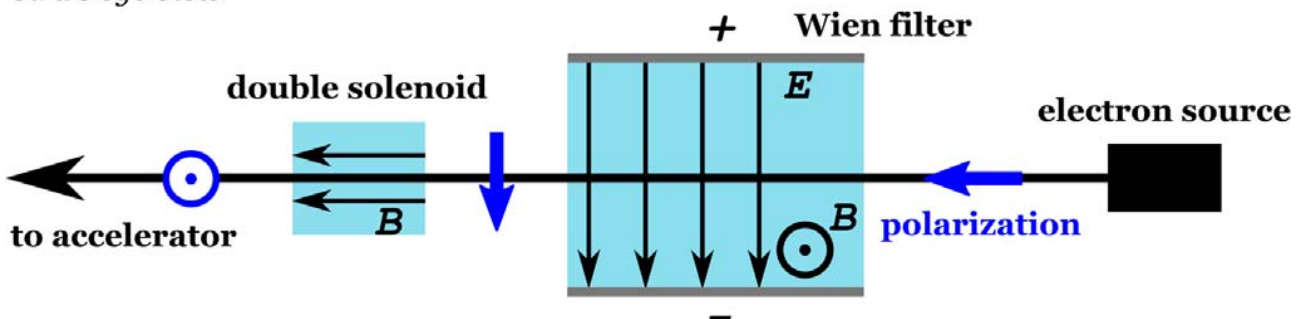


Figure 3.2: Setup for the trasverse polarization.

Following the picture, the longitudinal polarized electron from the source are rotated first in the XY plane, to obtain the trasverse polarization, then with subsequent double solenoid the spins are rotate in the vertical direction. After this allignment the electrons go through the accelerator to the experimental hall. The spins

then precesses during this time in the magnetic fields of the accelerator's bending magnets, following the BMT equation. In our experiment, because of the vertical polarization, only the residual horizontal component precedes during the motion. For conventional experiment the polarization vector is rotated by the Wien filter with an angle such that the polarization is longitudinally aligned in the experimental hall, considering that after the rotation, the polarization is affected by another rotation due to the spin precession. The rotation angles of the polarization vector through the accelerator are known from simulations and are also directly measured for relevant energies, for a beam of 570 MeV the rotation angle is 55° with an accuracy of ±2° At the beginning MAMI was not developed with the aim a trasverse beam. So it's not possible to measure directly the polarization for the vertical axis. However it's possible, with the existing setup, to exstimate the degree of polarization. For this purpose a Moller, Comport and Mott polarimeters are used. The vertical polarization alignment can be accomplished by the minimization of the horizontal components.

### 3.2.3 Polarization measurement.

#### Briefly explain how the Mott polarimeter works, for measuring the polarization of the beam.

To Measure the polarization of an electron beam different polarimeters can be used. Here we explain briefly the physics underlying the *Mott* polarimeter, used in the experiment. Consider an electron beam that is sent towards a nucleus of charge  $Ze$ . We know from theory that the spin of the incident electron is affected by the electromagnetic field produced by the nucleus. This can be described as:

$$\vec{B}_{nucleus} = \frac{-1}{c} \vec{v} \times \vec{E}_{nucleus} = \frac{Ze}{mcr^3} \vec{L}$$

$$V = -\mu \cdot B_{nucleus} = \frac{Ze}{mcr^3} \vec{L} \cdot \vec{S}_{e^-}$$

We can recognize the spin-orbit interaction here. This term yields the polarization dependence of the cross section. The cross section can be model in the following way

$$\sigma(\theta) = I(\theta)[1 + S(\theta)\vec{P} \cdot \vec{n}]$$

Here a scheme to identify the scattering process:

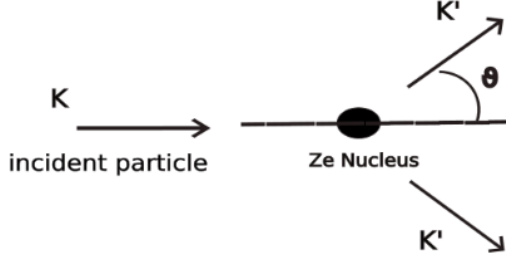


Figure 3.3: Scheme of the Mott scattering, the polarization is ortogonal to the plane,  $\vec{n} = \frac{\vec{k} \times \vec{k}'}{|\vec{k} \times \vec{k}'|}$

The direction of  $\vec{n}$  dependso on whether scattering to the left or right is being considered. Let's suppose our initial beam has a polarization  $P$ , and so we compute the asymmetry  $A(\theta)$  of the scattered electrons between left ( $N_L$ ) and right ( $N_R$ ).  $N_L$  and right  $N_R$  will be proportional respectively:

$$N_L = N_\downarrow[1 + S(\theta)] + N_\uparrow[1 - S(\theta)]$$

$$N_R = N_\uparrow[1 + S(\theta)] + N_\downarrow[1 - S(\theta)]$$

$$A(\theta) = \frac{N_L - N_R}{N_L + N_R} = \frac{N_\downarrow(1 + S(\theta)) + N_\uparrow(1 - S(\theta)) - N_\uparrow(1 + S(\theta)) + N_\downarrow(1 - S(\theta))}{N_L + N_R} = \dots = P \cdot S(\theta)$$

From the last equation we have a relation which give the beam polarization in terms of  $A(\theta)$  (which is what is measured) and the asymmetry function  $S(\theta)$  (known also as Sherman function). There are several calculation of the Sherman function, which is well-known for high energy electron scattering.

The total beam polarization is measured by a Moller polarimeter, in the experimental hall, with the beam polarization oriented longitudinally in the experimental hall. The Moller polarimeter can measure the longitudinal polarization of the beam.The other two polarimeters, Compton and Mott, located behind the injector linear

accelerator (ILAC), are sensitive to the longitudinal and the trasverse horizontal components of the beam (with an energy around 3,5 MeV at this stage). The procedure for the alignment is the following: at the beginning of the beam time the Mott polarimeter is used for different settings of the solenoidal field, with the Wien filter angle equal (nominal) to  $90^\circ$ . The aim is to minimize the horizontal polarization component after the rotation performed by the double solenoid, changing the solenoidal magnetic field. Then a second optimization follows, using the Moller polarimeter for different Wien filter angles is performed. With the new Wien filter settings, another measurement is performed with the Mott polarimeter.

### 3.3 Experimental hall setup.

Describing the A1 room, how the spectrometers are operating (+ figures), a picture of the target and the important parameters, like thickness. Also mention the convention to use target with 10% of the radiation length, to avoid double scattering. Mention that we need the Wobbler magnet to change the hitting position of the beam to prevent the target from melting. Here it's important to mention that the electrons are deflected in the vertical direction, because of the high beam intensity. Then add a picture of the beam-line.

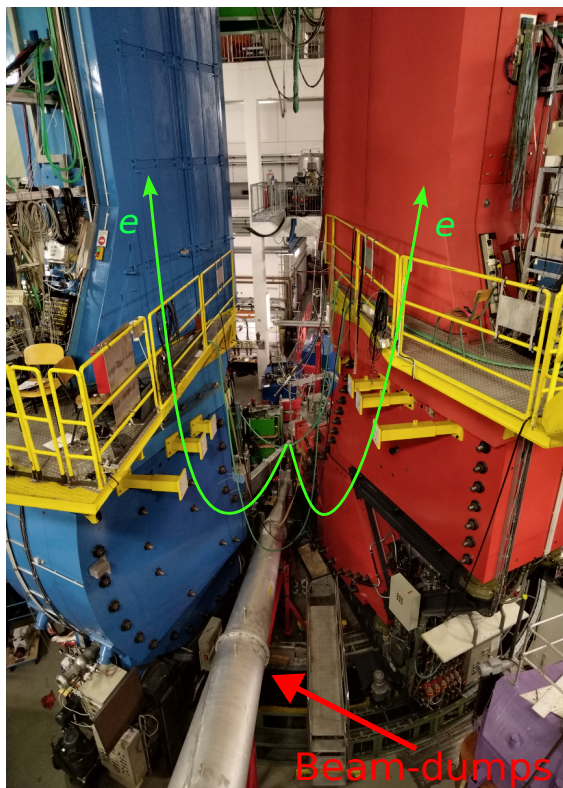


Figure 3.4: Picture of the A1 spectrometers hall. The spectrometers are the blue and red detectors on the left and right. The detector can be rotated using a system of railtracks that are visible at the bottom of image. The electrons are scattered and then deflected in the vertical direction by the magnetic field (green lines). This picture is taken from behind the target, so we see the beam-dumps. The target is roughly at the center of the image where the two green lines join.

### 3.4 Detectors and beam monitors

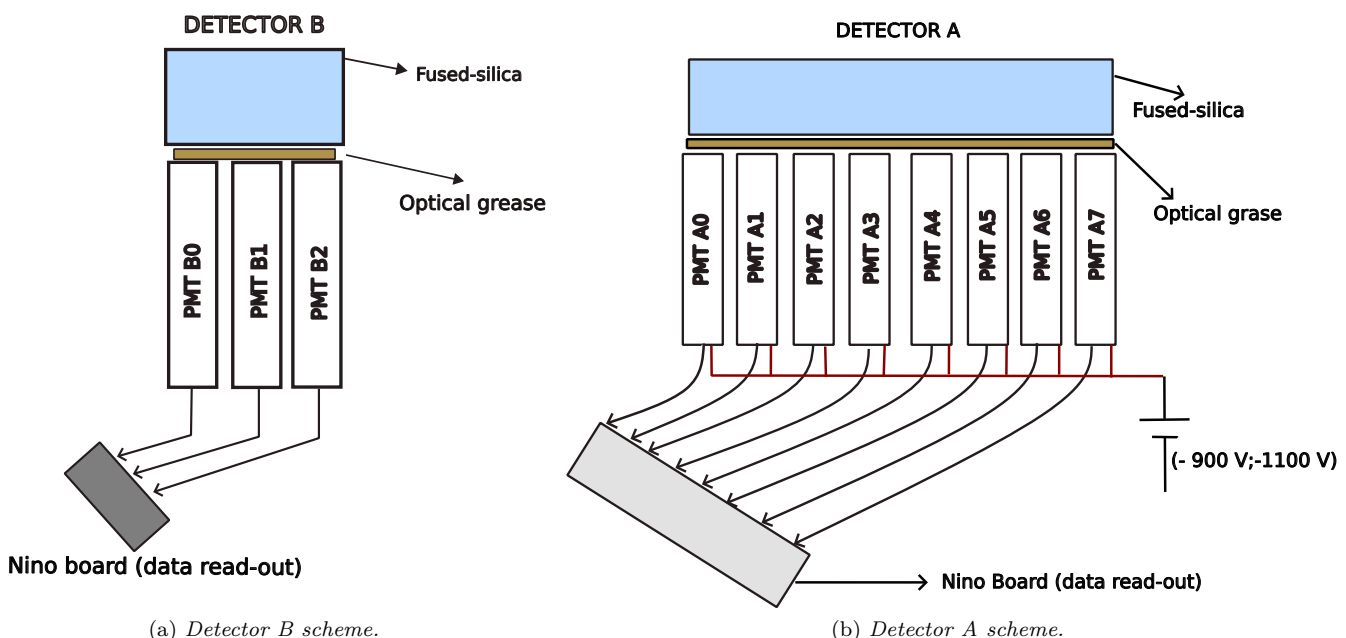
#### 3.4.1 Detectors A and B

Describe the two detectors we placed inside the spectrometers, the  $Q^2$  for our measurement. The way the counts are collected, so the expected signal for the Čerenkov detector. Explain also how we will use the old detectors of the two spectrometers to align the elastic scattering plane to our detectors.

- explain the two detector, the type of cristal used.
- how the pmt are coupled to the cristal, the number of dynodes of the pmt, the power supply.
- add an picture/scheme of the pmt.
- explain why a diffusor is not needed.
- what kind of optical coupling is used?
- dimensions of the two detectors.

In this section we will describe the electronics and the detectors used to measure the transverse asymmetry. For this experiment we are going to measure the transverse asymmetry at different angles. The electrons detection is made via two thin blocks of fused-silica that are coupled to PMTs. When a scattered electron hits the fused-silica (refractive index  $n = 1.45$ ) Cherenkov light is emitted. The emitted Cherenkov light can interact with the electrons of the material, which, in turn, can hit the PMT diode. This sequence of events triggers the PMT and produce an output signal.

In the experiment, we will measure the transverse asymmetry at two angles of scattering, so two detectors are installed and read-out independently. The two detectors are made by 3 PMTs and 8 PMTs coupled with two blocks of fused-silica, a scheme of the detector is shown below:



These two detectors are placed inside the spectrometers presented in aggiungere referenza, between the top of the drift-chamber, which occupies the first third in height of the spectrometer, and just below a panel of scintillator. During the beam time the drift chamber of the spectrometers is turned off, and also the PMTs coupled to the spectrometer scintillators are not powered.

As we mentioned above, the scattered electrons are deflected in the vertical direction by the magnetic field of the spectrometer. This is not common for an particle accelerator. The reason is due to the high intensity beam that can produce a strong noise, if the detector are placed too close to the scattering point (**magari è meglio chiede ad Anselm, perchè non posso liquidarla in due righe così**).

At this moment, it is important to mention the differences between the new and the old electronic setup. In the old electronic setup the output signal of the PMTs was integrated during the time interval of each sub-event, and therefore the single scattered electron could not be counted. The advantage of this method is that the electronics is more simple, in fact there is no need to develop a fast counter, unlike the new setup, where the new electronics take into account of every pulses. However, this old method is effected by a baseline noise and it's not good for the future experiments with lead target, where the expected rates are lower than the rates on carbon. With the new electronics, all the single electrons are counted, and this will allow the future measurements with lead, improving the accuracy.

Here we report the characteristic of the two detectors that are relevant for the data analysis:

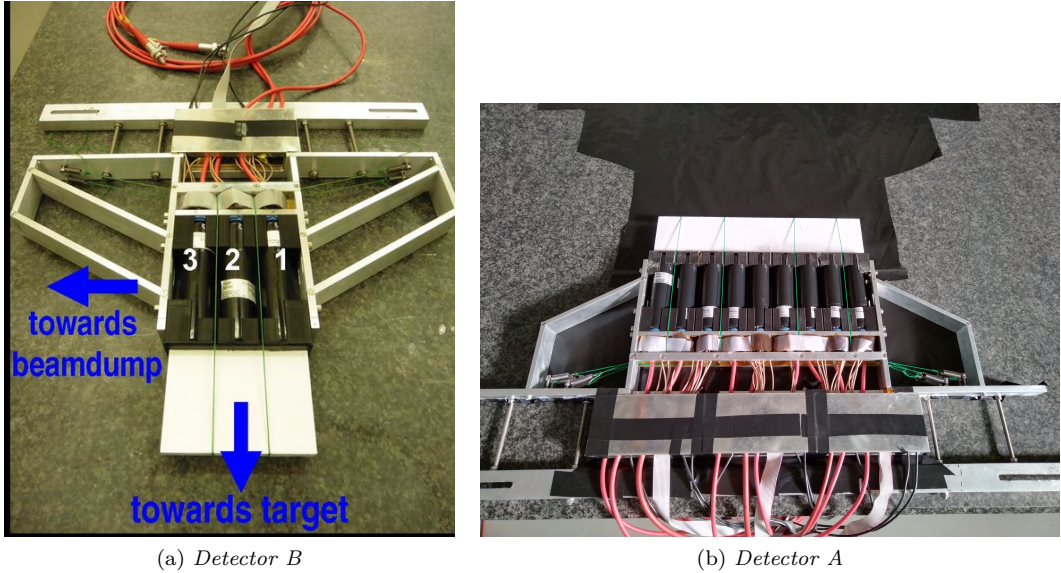


Figure 3.5: Picture of the two detector taken in the clean room. The white blocks are the fused silica that produces the Cherenkov light, the cylinders below are the PMTs.

- detector B size:
- detector A size:
- Number of dynodes:
- Voltage :
- refraction index  $n$  of the fused-silica:

The fused silica size for detector B is (7 cm, 10 cm).

### 3.4.2 Beam monitors.

**Explain how the monitors for the beam parameters work. (this section could be long, however the way these parameters are measured is particular, so it's important to explain everything properly).**

In MAMI, several monitors are placed along the beam line in order to check beam quality and measure parameters such as current intensity, energy and relative position of the beam. This section summarize an explanation of the operating principles of the monitors installed at MAMI. The explanation will be partial, some details will be given in the appendix, however for a complete discussion please refer to the following paper ([2]).

The monitors available at MAMI are quite specific for the standard of the particle accelerators. Resonant cavities are used to measure the various quantities, with the underlying physical principle that the passage of charged particles through these cavities can excite some electromagnetic resonant modes<sup>1</sup> which can be detected and analyzed by an analogic circuit to measure the beam parameters. Before going into the details, is necessary to define some quantities that will be used later in the explanation. We define  $r_s$ , the Shunt-impedance as :

$$r_s = \frac{|V_{||}|^2}{P} \quad (3.2)$$

$P$  is the power absorbed by the cavity when a particle excites one of the resonant mode, instead  $V_{||}$  is defined as the effective voltage surpassed by a charged particle along a straight line, which can be computed as:

$$V_{||} = \frac{1}{q} \int_{s_0}^{s^1} \vec{E}_s \vec{e}_s ds$$

---

<sup>1</sup>TM mode, where the magnetic field is completely transverse respect to particle momenta

The Shunt impedance is a measure of the interaction strength between a cavity and a charged particle, and can be expressed also in another way, introducing the  $Q$  value of the cavity,  $W$  the maximum energy stored and  $f_r$  the frequency of resonance:

$$r_s = \frac{|V_{\parallel}|^2 Q}{2\pi f_r W}$$

When the beam travel through the cavity, the particles release enery that excites the oscillascion mode. The power  $P_{HF}$  extracted from the beam is related to the beam current:

$$P = i^2 r_s$$

An antenna is used to decouple part of the energy from the cavity and send it to a circuit which produces an analog output signal. Indicating with  $\kappa$  the coupling costant of the antenna, the previous relation need to be modified introducing a new factor  $\frac{\kappa}{(1+\kappa)^2}$ . In a Cylindrical resonator, the same type installed at MAMI, the resonance frequency of the different oscillascion modes is expressed by the formula

$$f_{m,n,p} = \frac{c}{2\pi\sqrt{\epsilon_r\mu_r}} \sqrt{(\frac{x_{m,n}}{R})^2 + (\frac{p\pi}{L})^2}$$

The costant in the formula are:

- $c$  is the light speed.
- $\epsilon_r, \mu_r$  are the magnetic and dielectric costant of the material.
- $x_{m,n}$  it the n-th zero of the m-th Bessel function.
- $R$  and  $L$  are the radius of the cylindrical cavity and his lenght.
- $p$  I dont' know yet.

This formula can be obtained solving the Maxwell equations with cylindrical boundary condition, the eigenvalues are the given by the formula above.

If the frequency of the Beam bunch is equal to the resonant frequency  $f_{m,n,p}$  of the cavity, a TM mode is excited. At MAMI high quality monitors are installed, quantitatively all the monitors have a  $Q \simeq 10000$ , that means that  $\frac{v}{\delta\nu} \simeq 10000$ . This means that the frequency of the beam bunch must be very close to the frequency of the resonant cavity. At MAMI the frequency used for all the resonators is 2,449 532 GHz or a multiple of it. The beam bunch frequency is the same, and it's controlled by the MAMI-master oscillation signal, that is the reference signal for all the MAMI monitors.

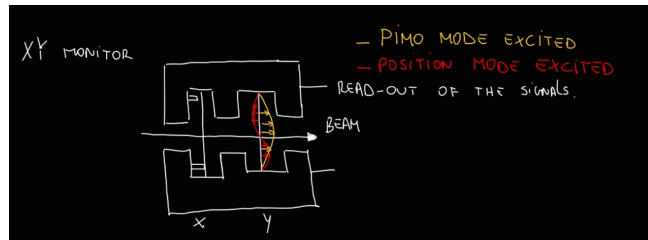


Figure 3.6: Scheme of the Cylindrical cavities installed at MAMI. In red we have the  $TM_{110}$  mode, used to measure the position of the beam, in yellow the  $TM_{010}$  mode, to measure the intensity of the beam.

Depending on the  $TM$  mode excited, we have a different signal in the cavity, so a different signal collected by the antenna. The relevant quantity that is detected is the power  $P_{HF}$  absorbed by the antenna. For the  $TM_{010}$  mode, the power is

$$P_{HF} = i^2 r_{010} \frac{\kappa}{(1 + \kappa)^2} \quad (3.3)$$

The power absorbed by the antenna is directly dependent on the beam current. Because the rage values are typically in the range of pW to mW, the signal is processed in close proximity of the installed monitors. In the

signal process, the input signal of the antenna is coupled to the master-oscillation signal, so the output signal is given by the formula:

$$U = \sqrt{P_{HF}} \cos(\phi - \phi_{LO}) \quad (3.4)$$

the phase  $\phi$  is the phase of the resonant mode or the phase of the beam bunch, while the phase  $\phi_{LO}$  is the phase respect to the master-oscillation signal, and can be adjusted by a phase shifter of the circuit. The output voltage signal can be read out with the oscilloscope or digitalized and saved with other devices. To measure the beam intensity is important to minimize  $\phi - \phi_{LO}$ , to maximixe the signal amplitude, and then the output signal is ready to be analyzed.

The measurement of the  $x, y$  position follows in principle the same procedure. In this case the  $TM_{110}$  is acquired. The reason is clear, because it's possible to calculate that for this mode the  $r_{shunt}$  is proportional to the beam position on the  $x, y$  plane. So The power absorbed by the antenna can be written:

$$P_{HF} = i^2 r_{110} \frac{\kappa}{(1 + \kappa)^2} Kx^2 \quad (3.5)$$

with the output signal prortional to the square root of the absorbed power, we end with:

$$x, y = \sqrt{(P_{HF})} = costant \cdot \frac{U}{i} \quad (3.6)$$

With this is clear how it's possible to measure all the important quantity related to the beam that will be used for the analysis.

### 3.4.3 Beam stabilization.

## 3.5 Electronics

**Short introduction about the old electronics setup and why a new versions is needed, then describe all the electronics used for our experiment:**

- Nino board for collecting the data from the pmts
- VFCs for collecting the data from X21,X25,Y21,Y25,ENMO,I21,I13
- master board for collecting the monitors data/controlling the source/wobbler magnets.
- small boxes for switching from new electronic read-out to the old electronics read-out (spectrometers DAQ)

### 3.5.1 VFCs

Some parameters which describe the beam are needed in order to take into account possible effect in the measure of the Trasverse asymmetry. The relevant data are the position in the  $(x, y)$  plane, the incident angles on the target, the current and energy of the beam. All this values are collected using the already existing monitors. To collect the data from the monitors, single and multichannel, synchronous voltage-to-frequency converters (AD7742) are used. This devices contain an analog modulator that is able to convert the input voltage into an output pulse train, whose frequency is proportional to the input voltage.

The VFCs are powerd with an external tension of 5 V, and a differential voltage input in the range  $(-V_{ref}, V_{ref})$  is also applied. An external clock signal, that is indicated with "CLKIN" is provived as a reference signal for the oscillator frequency. The analog input signal is sampled with by a switched capacitor, with a rate that is controlled by clock that can be supplied externally, in our case we used a 6 MHz. A scheme of the electronic circuit is drawn here (*aggiungere figura*), the output of the Comparator is a fixed width pulse (the pulse is initiated by the edge of the clock signal) with a frequency that goes from  $0.5\% \cdot f_{CLKIN}$  to  $0.45\% \cdot f_{CLKIN}$  [1], where the first correspond to 0,0 V in input and the second to  $V_{ref}$ . Neglecting possible systematic errors, the relation the output frequency and the input voltage is the following:

$$V_{in} = \frac{V_{ref}}{40\% \cdot f_{CLKIN}} (f_{out} - 5\% f_{CLKIN}) \quad (3.7)$$

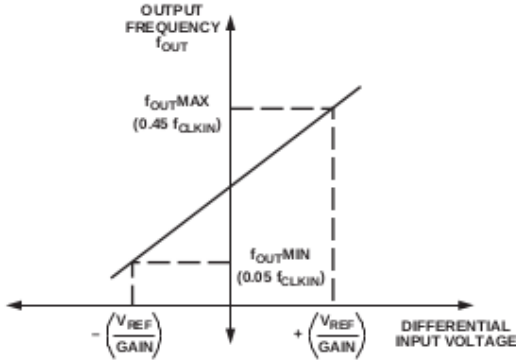


Figure 3.7: Frequency versus Voltage

differential signaling (LVDS). Each comparator can handle eight channel and for each of them it is possible to define a global threshold. With the current settings of NINO board, it is possible to change the threshold of each channel acting on another value, the attenuation, which decreases the value of the global threshold of each single channel. All the value that can be modified are 12 bit numbers, so a setting interval of (0.; 4095).

We control the  $f_{CLKIN}$  with the period of the clock. The data are acquired counting the number of pulses that come from the comparator, so we can substitute to  $f$  the number of pulses (the two quantities are proportional), and we end with:

$$V_{in} = V_{ref} \left[ 2 \cdot \frac{N_{pulses} - 5\%N_{CLKN}}{40\%N_{CLKN}} - 1 \right] \quad (3.8)$$

### 3.5.2 Nino board

The NINO board is our data acquisition system for the pmt counts. It is made by 32 analog input channels and it's power with  $\pm 5$  V. Each channel has an attenuator, and the signal pass through that before going to the Comparator, which compare the signal to the threshold. The Output signal is a Low-voltage

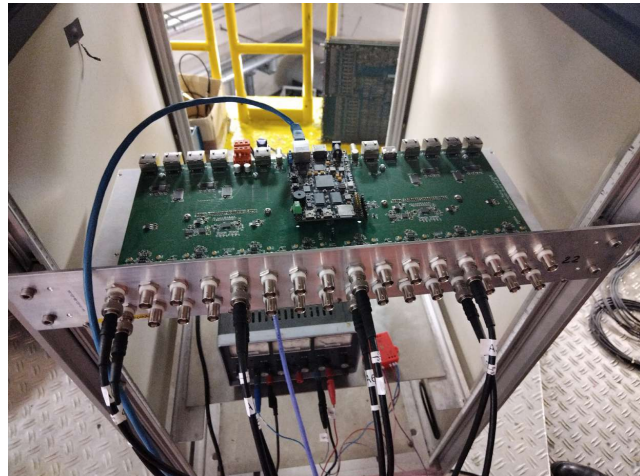


Figure 3.8: Nino Board

Two Nino board are used in the experiment, one for detector A and one for detector B. In principle it is possible to use only 8 and 3 of the 32 channels the are ready to use, considering we have only 3 and 8 pmts to read out. However it is useful to split the analog output signal by the pmts and send it to 4 different channels. So, working with the attenuation value, we can define 4 different threshold values for each pmt. This is something that can improve the noise management. This will be implemented for the future experiments, nevertheless this was not done during our data collection. The way we selected the threshold is explained in the following chapter (Analysis).

### **3.5.3 Master Board**

# Chapter 4

## Detectors Test, alignment and calibrations.

1. development of the analysis program.
2. testing the analysis program with montecarlo data.
3. Test of the detectors in the Lab.
4. Beam line description.
5. Data Analysis
  - (a) thresholds scan
  - (b) Rates on  $Pb^{208}$ .
  - (c) Beam related asymmetry correction.
  - (d)  $C^{12}$  Asymmetry.

**Introduction** In this chapter we discuss the electronic test that have been carried out in the laboratory, and the calibrations that need to be done in order to calculate, from the raw data, the final data ready for the analysis. The test in the lab consist in checking that the photomultipliers are working and that the electronics that take care of acquiring the data do not have any errors. For the calibrations, since several beam parameters are needed for the analysis, it's importat to obtain the correct scaling factor to convert the Raw Data collected by the *VFCs* to data with the right physical units, as the  $X, Y$  impact point of the beam on the target, the beam energy  $E$ , the beam currer  $I$  and the scattering angles  $\theta_x$  and  $\theta_y$ .

### 4.1 Data tree

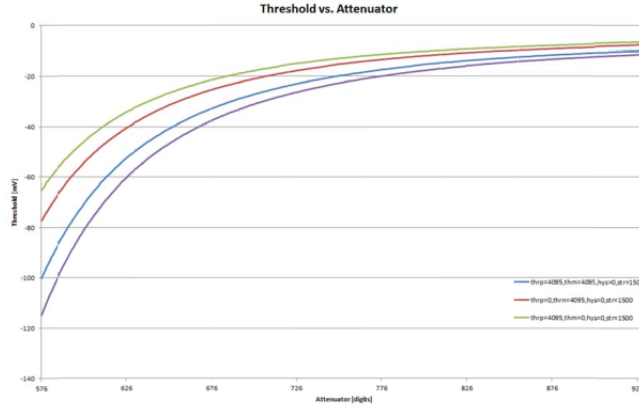
Explain how we compute all the values for the data tree, the position of the beam on the target, the angle, the correlated-difference values...

### 4.2 Detectors test

Explain the test of the two detectors in the lab, how we select the threshold, the correlation of the pmts and coincidence to select the threshold. Mention also that we observed two knees in the plot of counts vs. attenuation.

The Nino board, which digitizes the signal from the PMTS, has two parameters which can be used to select the internal threshold of the discriminator, to cut the low amplitude signals and can be adjusted changing the settings of the DAQ program. These two parameters are *Threshold* and *Attenuation*. *Threshold* means directly the charge value necessary for an impulse certain shape to be accepted by the signal discriminators. However the "physical" threshold can be also modified changing the *attenuation*. The relation between threshold and attenuation is not linear, but follows:

For our purposes, we select a common threshold values for all the pmts, and we decided to change only the attenuation values.

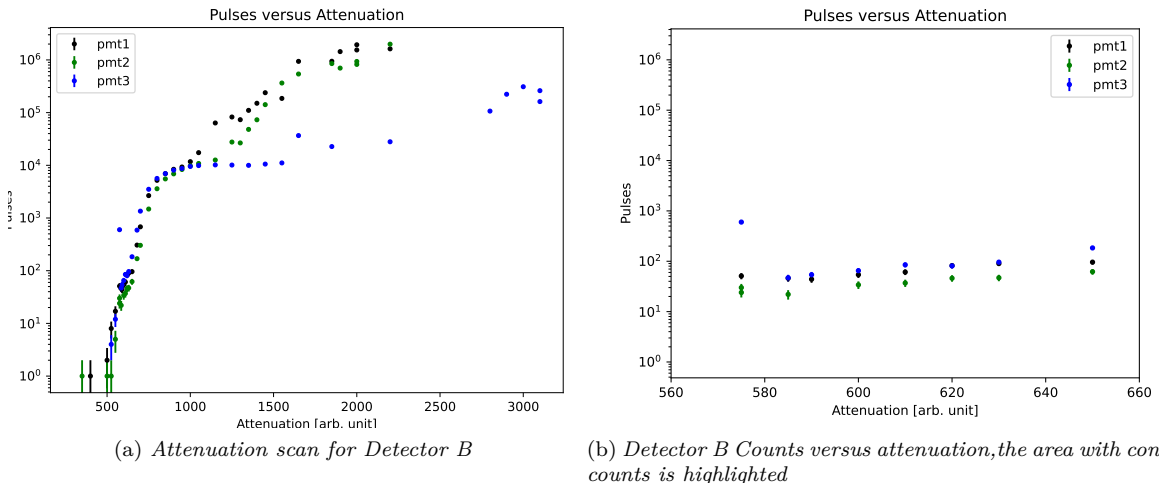


(a) Threshold dependence against attenuation

Before the Beam time, some test with the two detectors were performed, to check that the pmts were still working after some years of inactivity, and that the new electronic was able to count properly the pulses and store the data. For this studies, we didn't have a radioactive sources to employ, so we moved the two detectors in the workshop of the accelerator, and we use the cosmic rays rate as a probe.

Knowing that the expected number of event for cosmic rays is about  $1 \frac{\text{event}}{\text{cm}^2 \text{s}}$  we can compute the expected values for the number of events. We decided to take 1 minute long acquisition for both the two detectors, this leads to 70 expected events for detector B and 100 events for detector A.

The first step is to select a good point of work for the threshold. So, fixing the value of the threshold parameter for the NINO board, we took several acquisitions, each of them one minute long, increasing each time the attenuation. We powered the pmts with a negative voltage around  $-1000 \text{ V}$ , as suggested in the datasheets, and covered the cherenkov detector with a shielding blanket, to avoid ambient light simulating a signal.



(a) Attenuation scan for Detector B

(b) Detector B Counts versus attenuation, the area with constant counts is highlighted

We observed a small knee in the plot, around the zone of  $580 - 600$  of attenuation, where the number of counts was almost constant, roughly equal to the number of expected events from muons hitting the detector. Then we observe a big edge for attenuation = 1000. Looking at the plot 4.1a, we assume that the attenuation values are so high that electronic noise is no longer rejected, in fact the counts grow enormously. The attenuation was set at 600.

The next step was to study the statistical fluctuation of the counts, so we collected 10 acquisitions, each of them 1 min long. The measured values are reported in the table below:

Pmt:	1	2	3
1	58	60	62
2	62	55	59
3	61	59	70
4	73	66	70
5	68	66	56
6	59	52	64
7	69	74	77
8	48	49	57
9	70	54	58
10	60	61	66

This data are interesting to check if the counts are following the theoretical distribution of the events expected for cosmic rays at sea level. If the pmt are working in a good mode, we know that the number of counts should be Poisson-distributed:

$$Pdf(\mu, k) = \frac{\mu^k}{k!} e^{-\mu} \quad (4.1)$$

The variance of the poisson distribution is equal to the mean of the counts, and we expect the same behaviour also for the sample mean and the sample variance:

$$\begin{aligned} \mu_1 &= 62.8 & \sigma_1^2 &= 54.40 & r_{12} &= 0.66 \\ \mu_2 &= 59.6 & \sigma_2^2 &= 57.15 & r_{23} &= 0.65 \\ \mu_3 &= 63.9 & \sigma_3^2 &= 46.98 & r_{13} &= 0.35 \end{aligned}$$

We report also the correlation  $r_{xy}$  between the pmt. The result are fine: we are able to see a positive correlation between adjacent pmt, and as expected the correlation is lower in the case of the more distant. This is explained by the lower probability that the photons of Cherenkov radiation light up at the same time the more distant pmt. We can test that the data follow a possion distribution using the well-known Gosset test, defined as:

$$\chi_{n-1}^2 = \sum_{i=1}^n \frac{(Oss_i - Att_i)^2}{Att_i} \quad (4.2)$$

We report the result obtain with the data for detector B, the test shows that there is good agreement with the hypothesis that the count are really poisson-distributed.

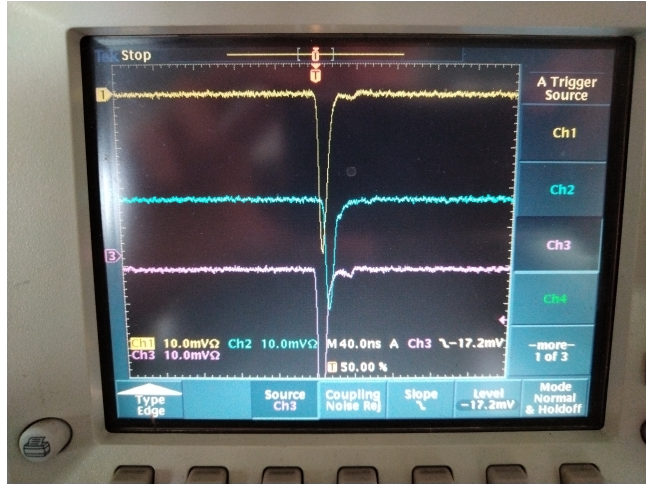
Pmt:	1	2	3
$\chi_9^2$	8.52	8.45	6.37

To convince oneself that the pmt are actually measuring signals given by the passage of cosmic rays, and not noise, we exploit the possibility of we exploited the possibility of placing one pmt in coincidence with the others. If we are able to observe correlation between the counts, we can conclude that the detection electronics are working correctly.

One pmt was placed over the detector and we read out the counts simultaneously.

pmt	0	1	2	4 (in coincidence)
1	63	57	72	28
2	55	51	64	18
3	62	53	75	27
4	71	62	75	33
5	68	59	49	23
6	57	55	63	18
7	70	64	64	24
8	50	69	69	25
9	65	62	62	19
10	74	71	77	28

As above, we report the sample mean, the variance and the correlation between the pmt in coincidence and the detector B:



$$\begin{aligned}
 \mu_0 &= 63.5 & \sigma^2 &= 58.9 & r_{04} &= 0.49 \\
 \mu_1 &= 60.3 & \sigma^2 &= 43.3 & r_{14} &= 0.38 \\
 \mu_2 &= 67.0 & \sigma^2 &= 71.1 & r_{24} &= 0.65
 \end{aligned}$$

We observe a positive correlation  $r_{04}, r_{14}, r_{24}$  for the pmt in coincidence, this is a strong evidence that the signals are correlated and that some particles are hitting the fused silica sequentially.

Pmt:	1	2	3	pmt in coincidence
$\chi^2_9$	8.95	6.44	10.96	9.52

We also check at the oscilloscope if we were able to observe three negative peaks at the same time:

The same procedure was followed also for detector A, made by 8 PMTs. We analyzed 4 pmt at a time, having the NINO board available with only 4 channels. The same attenuation scan performed for detector B was done:

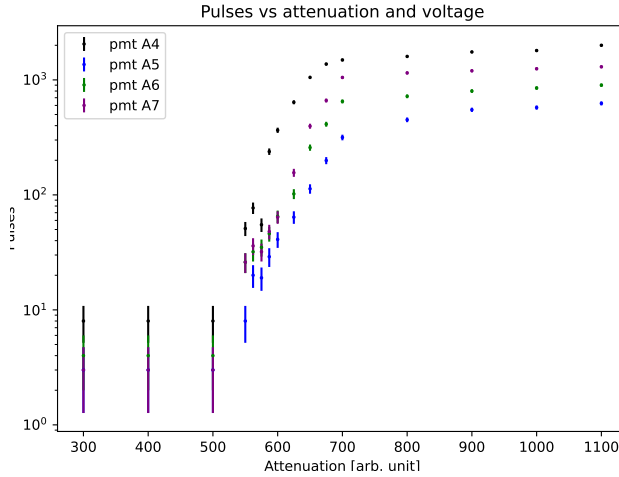


Figure 4.1: Attenuation scan for Detector A

For these 4 pmt we are able to observe

We took as above 10 acquisitions 1 minute long:

pmt	2	1	0	4 (in coincidence)
1	91	51	50	27
2	86	61	50	7
3	58	48	45	18
4	95	62	41	29
5	69	60	50	21
6	85	57	45	19
7	66	51	46	28
8	74	51	48	22
9	77	43	45	17
10	62	44	50	29

$$\mu_2 = 76.3 \quad \sigma^2 = 160$$

$$\mu_1 = 52.8 \quad \sigma^2 = 47.5$$

$$\mu_0 = 47.0 \quad \sigma^2 = 9.6$$

$$\mu_4 = 21.7 \quad \sigma^2 = 48.2$$

For these 4 pmts , the variance of the sample changes significantly from what was observed earlier. We report in this table the correlation matrix:

pmt:	4	0	1	2
4	1	-0.18	-0.21	-0.06
0	-0.18	1	-0.10	-0.22
1	-0.21	-0.10	1	0.56
2	-0.06	-0.22	0.56	1

Here we observe correlation that with negative sign, which are not expected. Also the correlation between the pmt in coincidence are negative. If we try to perform a gosset test, we obtain:

Pmt:	2	1	0	pmt in coincidence
$\chi^2_9$	19.6	8.30	1.90	39.5

The expected error for the result of this test is  $\sigma = \sqrt{2 * (n - 1)} \simeq 4$ . In this case we are observing 3 values that are  $2 \cdot \sigma$  far from the expected value. All this consideration indicate that the attenuation, or something in the DAQ program is not correctly set.

## 4.3 Calibrations.

One of the main goal for this experiment was to measure the well known trasverse asymmetry of  $^{12}C$ , already measured before, as a test for the new electronic system. Previous measurements of the Transverse asymmetry have been performed for a carbon target. For this beam-time, the two spektrometers were placed at an angle such that the  $Q^2$  values of the scattered electron is:

<i>SpektrometerA :</i>	$Q^2 = 0,041\,337 \text{ GeV}$	without Cut
<i>SpektrometerA :</i>	$Q^2 = 0,039\,451\,3 \text{ GeV}$	with Cut
<i>SpektrometerB :</i>	$Q^2 = 0,040\,477\,1 \text{ GeV}$	without Cut
<i>SpektrometerB :</i>	$Q^2 = 0,040\,584\,3 \text{ GeV}$	with Cut

The  $Q^2$  values is the same of the last measurement performed at MAMI, and is measured with and without rejecting the inelastic electrons.

### 4.3.1 Alignment of the scattering plane

### 4.3.2 Calibration of the VFCs monitors

Maybe it's important to divide this sections in two different part: the first part where I explain the Vfc convert the input voltage signal to a digital signal. In the second part just mention how we tuned the resistences (for X,Y monitors directly at the output signal with the oscilloscope, while for I21 and I13 monitors we used the data, so I'm able to produce plots only for the second ones).

### 4.3.3 Calibration of the PIMO monitors

For the calibration of the X Y monitors, we used two target made by three carbon wires at a certain distance from each other, aligned horizontally and vertically. The distance between the two center of the external wires is  $d_{horizontal} = 2,38 \text{ mm}$  for the target alligned horizontally and  $d_{vertical} = 2,33 \text{ mm}$  for the other one. When the horizontal wires target is cetered, we turn on the beam, and we take some data slowly changing the horizontal beam direction. The beam direction is changed by MAMI operators, varying the Magnetic field of the *Wobbler 16* magnets (4.2):

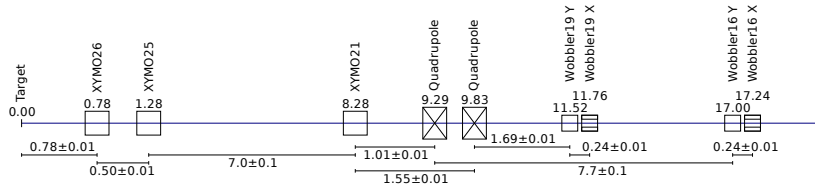


Figure 4.2: Beam line scheme.

Then we repeat the same procedure with the other target, for the vertical direction. We observe that the pmts counts increase to a maximum, that is reached when the beam spot is centered on the carbon wire, and

then decrease until the next carbon wire is hit by the beam.

We plot the pmt data *versus* the  $X_{25}, X_{21}, Y_{25}, Y_{21}$ , given in V. Given that we know the real distance between the two external wires, we can obtain the correct scaling factors to calculate the X and Y position values of the beam. To identify the three peaks in of the carbon target, we fit the data using a gaussian model (see 4.3). The mean  $\mu$  represents the center of the wire, given in V. Looking at the Beam line, we assume that the beam travels in a straight line. Let's consider the *Wobbler 16* magnet the "0" of a coordinate system, with the z axis pointing to the target (left direction in the beam scheme). The Beam parameters are measured by the Monitors  $X/Y_{21}, X/Y_{25}$ , which are located at some distance respect to the target. Suppose we are working only with the  $Y_{25}$  monitor (the procedure is the same for the others). The Beam y position is described by:

$$y_{beam} = m \cdot (z - z_{wobbler16})$$

In the scheme 4.2 we easily compute the distance between the  $Y_{25}$  monitor and the *wobbler 16* magnet, so we have the slope  $m$ . The Position on the target is given by  $Y_{target} = m \cdot Z_{target}$ . With these simple equations then:

$$c_{Y_{25}} = \frac{d_{vertical}[\text{mm}]}{Y_{target}} \quad (4.3)$$

$c_{Y_{25}}$  indicates the scaling factor of the monitor. With these values the Analysis program compute the correct beam position, and from that the incident angles in the  $x, y$  directions, which are needed later for the analysis.

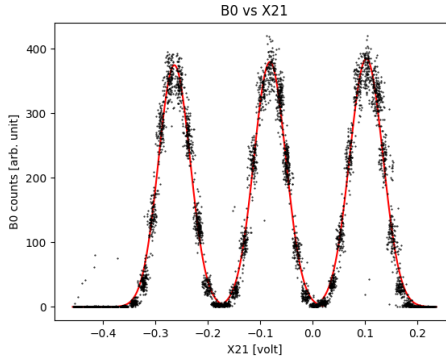


Figure 4.3: •

All this procedure can be easily checked if we plot now the  $X$  and  $Y$  position for the same two runs of data acquired with the wires. After placing the scaling factors obtained in the standard configuration file, we run the analysis another time and the physical values were computed 4.4

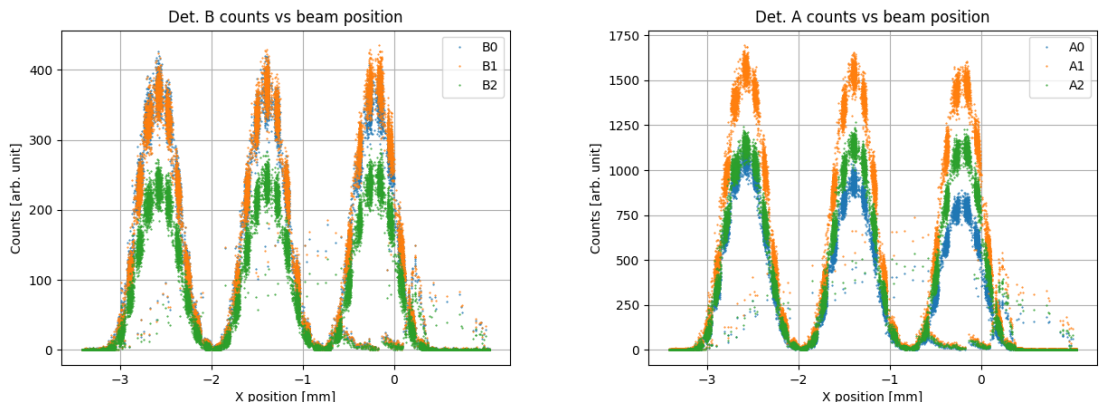


Figure 4.4: plot of the pmt Count against the physical values computed by the analysis program. Now the position of the three peaks correspond to the expected values measured for the target.

#### 4.3.4 Current (PIMO) and energy monitors (ENMO) calibration.

For the current monitors I13 and I21, we perform the calibration changing the current of the beam and observing the output values of the monitors (Voltage values). The we perform a fit (for the beam current, we used the nominal values that we communicate to MAMI, has the values for the x-axis).

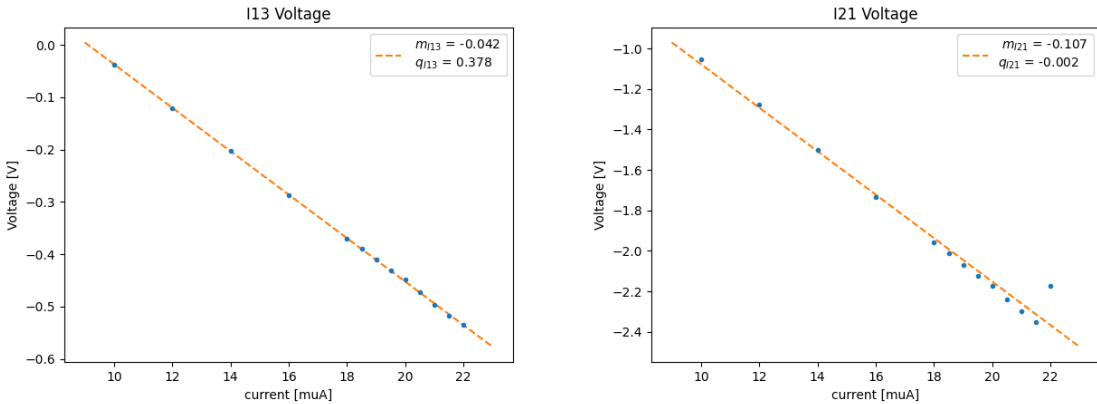


Figure 4.5: •

For the two monitors we are able to compute the offset and scale factor:

$$I_{13}^{volt} = m_{13} \cdot I_{13}^{Nom} + q_{13}$$

$$c_{13} = \frac{1}{m} \quad \text{offset} = -\frac{q_{13}}{m} \quad (4.4)$$

The same formula for current monitor I21.

The Enmo calibration is performed in a different way from the other monitors. The polarity signal is sent to MAMI, and they produce a signal for the ENMO that somehow (need to investigate exactly how they do that) shows a difference between the first two subevents and the last two. This difference is equal (nominal) to 22,6 keV. The idea now is to produce an histogram for the quantity  $\delta E$  (with  $E_{18}$  being the energy monitor):

$$\delta E = \frac{E_{18}[2] + E_{18}[3]}{2} - \frac{E_{18}[0] + E_{18}[1]}{2}$$

The data should be distributed with a peak around 22,6 keV. To obtain the correct scaling factor for the values stored in the data tree we plot the voltage values mesured by the ENMO monitor. 3 runs of data where taken with different Beam current, to study the dependence of the measured quantity from the beam current. From the mean of the distribution it is possible to exstimate the scaling factor for the ENMO monitors, obtaining the physical quantity in the following way:

$$C_{E18} = \frac{22,6 \text{ keV}}{\delta E}$$

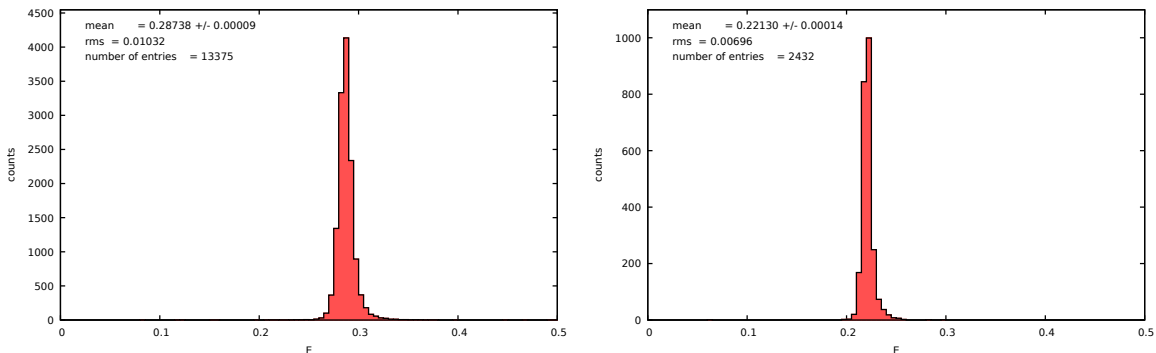


Figure 4.6:  $\delta E$  for 20 200  $\mu\text{A}$

Taking the average over  $E_{18}$  voltage values, and using the formula above, we obtain the coefficient  $C_{E18}$ . To take care of the current depencende of the monitors, the scaling factor to be placed in the standard.config

file is:  $C_{E18}\bar{I}_{\mu A}$ . The calibration was performed taking three short acquisitions with different beam current : 20  $\mu A$ , 15  $\mu A$  and a run without beam.

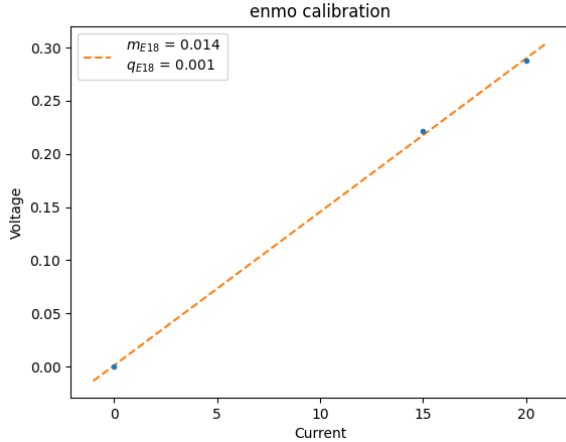


Figure 4.7: Calibration of ENMO monitor

From this we obtain the value  $scaling_{E18} = -1595.2$ , to obtain the physical quantity from the analysis. As a final check the final histogram for the physical quantity is shown:

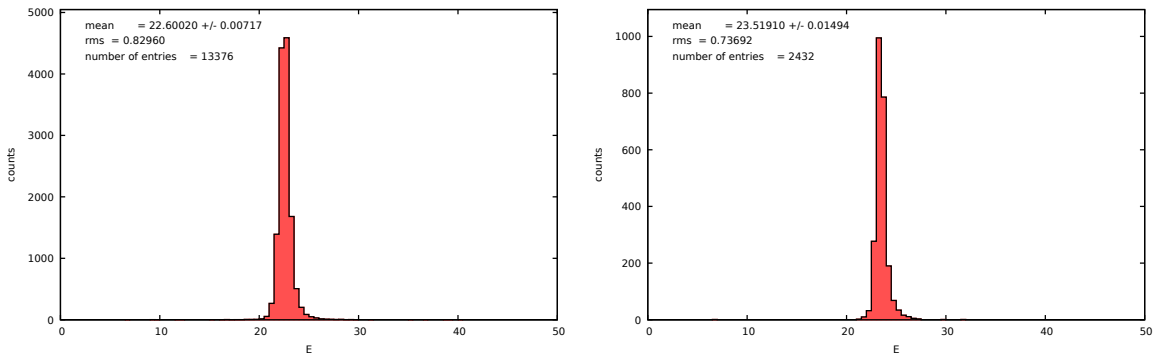


Figure 4.8: Plot for the physical quantities computed in the data tree, for two different current of the beam (on the left 20  $\mu A$ , 15  $\mu A$  on the right)

### 4.3.5 Calibration of the pmts

**Here it's important to show the plots I made during the beam time. I have to mention the Leo techniques for the correct interpretation of counts vs attenuation.**

During the beam time, several scans in attenuation were performed, before switching MAMI to produce the polarized beam, to choose the best working point for the PMTS of the detectors. The same procedure used in the laboratory was followed, starting from low attenuation and raising up the values. It's possible to get a simple model to describe the particular shape of the following plot taking into account simple assumptions about the type of electrical noise that affect the Nino board, and the *pdf* of the signal produced by the PMTS. The main assumption ("this is not a true assumption, Anselm has a plot of the digitalize charge that proves that") is that the signal amplitude, in mV collected by the Nino board is well described by a gaussian distribution, and for signal with low amplitude, we expect to be well described by an uniform distribution. Just to visualize, let's suppose that the distribution of the signal amplitude collected is of this type (4.9) (the following figure is just an example, the values do not describe the data collected):

The probability for a signal to pass the selection is equal to the probability of being in above the threshold, that is the complementary cumulative of the gaussian distribution (probability of being in the right tail):

$$P(signal > thr) = 1 - \Phi(x) = \frac{1 - Erf(\frac{x_{thr} - x_0}{\sqrt{2}\sigma})}{2}$$

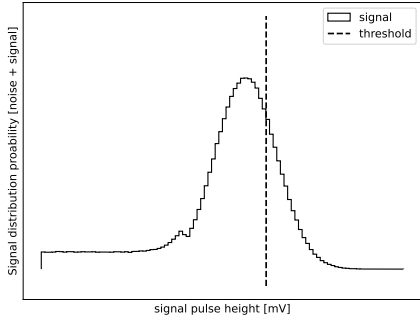
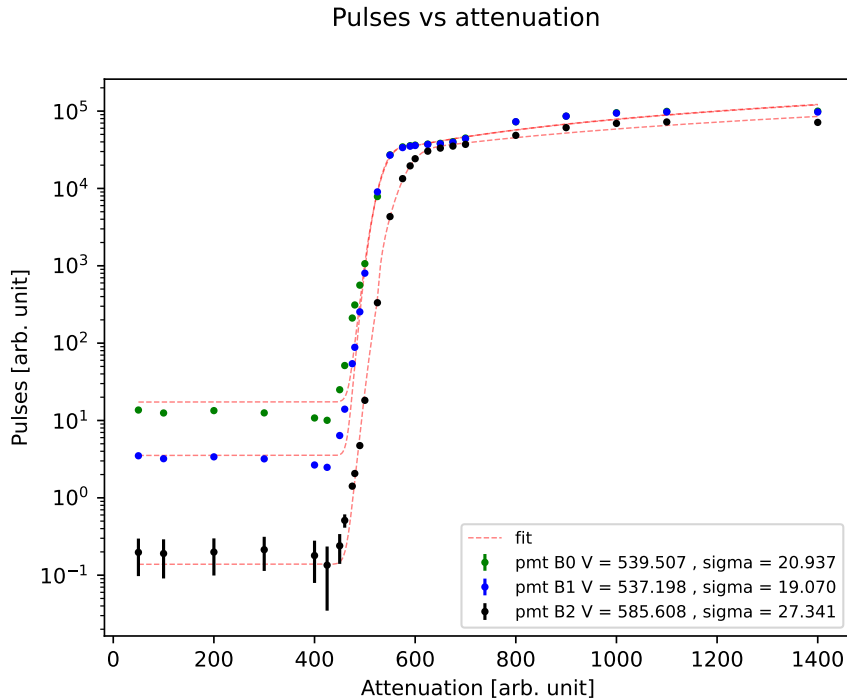


Figure 4.9: Example of the expected distribution of the PMTs output signal

Once we reach the uniform zone, the probability of an even being selected is proportional to the area of the rectangle, which increases linearly decreasing the threshold. Considering the normalization factor, it is straightforward to fit the data with a model of this type:

$$N(att) = N_0 \cdot \frac{1 + Erf(\frac{x_{thr} - x_0}{\sqrt{2}\sigma})}{2} \quad \text{if } att < C \\ N(att) = N(C) + m \cdot (att - C) \quad \text{if } att > C \quad (4.5)$$

For the detector B we show the result assuming our model:



(a) Attenuation scan for the pmts of detector B

From the fit we obtain three values for the signal Peak, given in attenuaton units. We can check the idea behind this, visualizing the pmt count in a different way. Because we would like to visualize the number of electrons that generate a certain signal in the detector, we can think of differentiating the data showed in the plot 4.10a. The differentiation consist in the difference between the Counts at a certain point and the previous one, and dividing by the increment in attenuation:

$$Spectra = \frac{N(att_i) - N(att_{i-1})}{att_i - att_{i-1}}$$

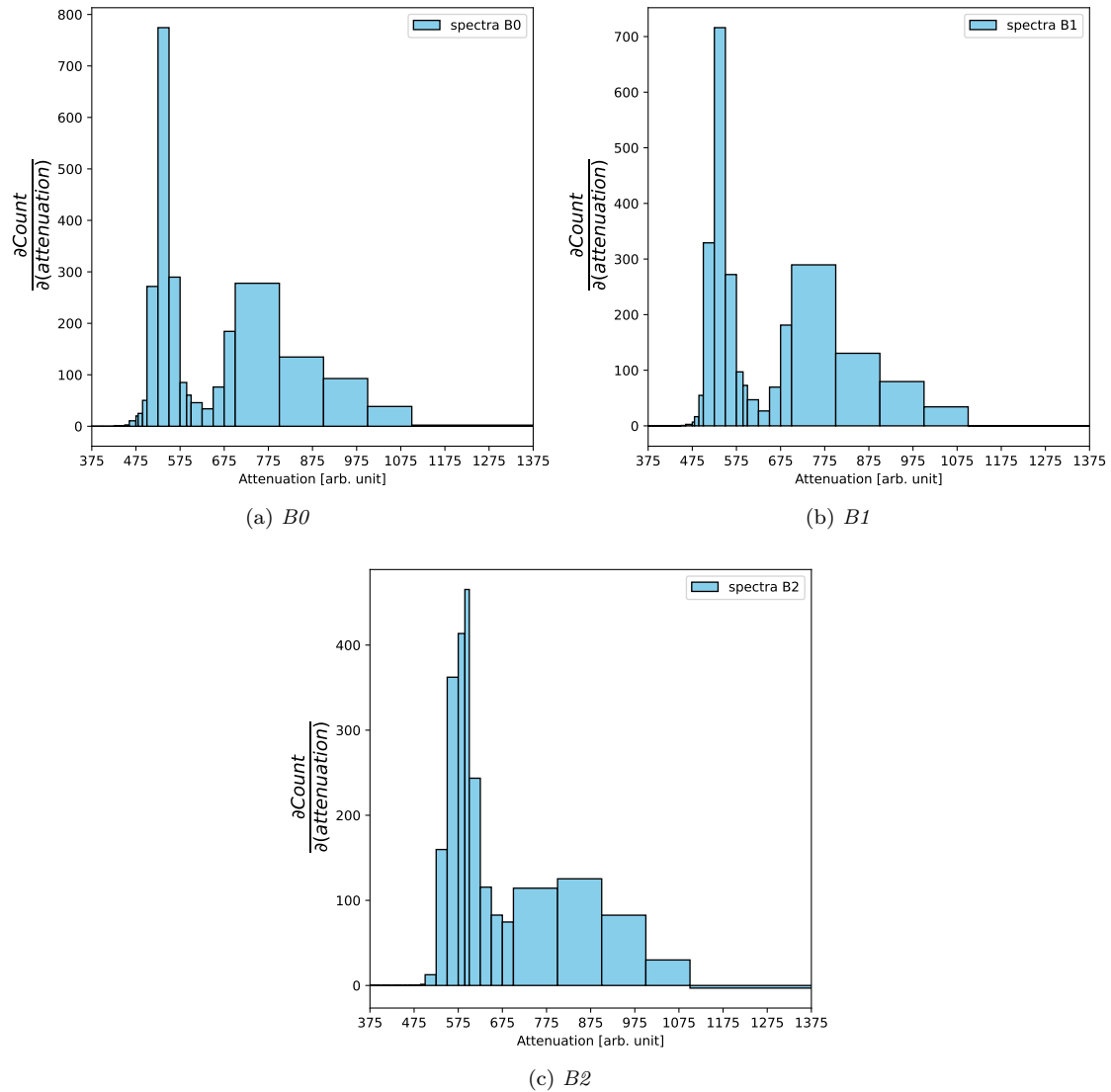


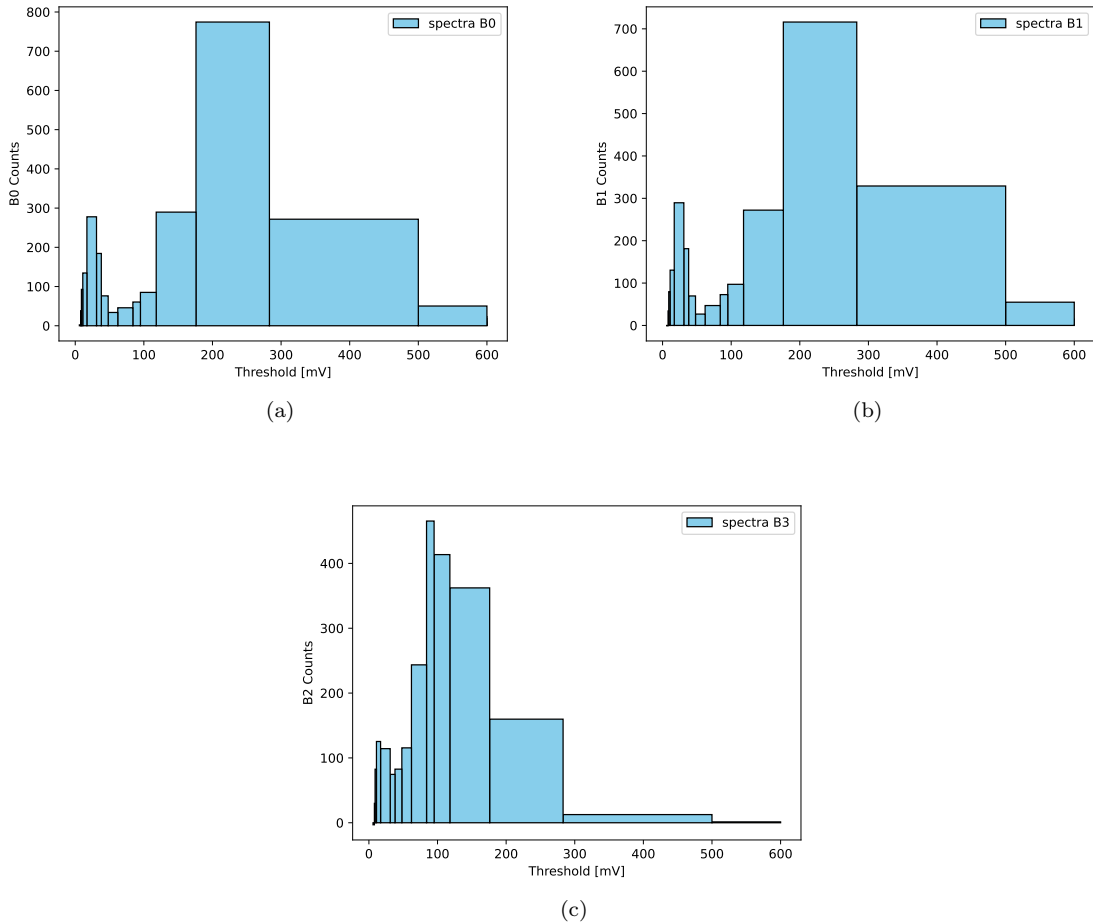
Figure 4.10: Reconstructed spectra for Detector B, notice that we have *Attenuation* values in the x axis, therefore right and left are swapped with respect to the graph 4.9.

In this way we compute a discrete derivative of the plot showed in 4.10a, which represent  $\frac{\partial N}{\partial att}$ . This is, in fact, the spectra of the signal, still given in attenuation units 4.10a.

This plot are used to identify a good point to select the attenuation values. If we look at the plot (), we can see that the physical threshold does not scale linearly with changing the attenuation value, and for high values of attenuation, the threshold falls quickly at zero. Looking at the signal spectra, we indentify the first peak as the electron signal, and the other peak for higher attenuation values (on the right), correspond to very low threshold values, so it is noise that we want to reject. We select the values of the attenuation downstream of the two distributions, taking all the pulses from the electron and rejecting rejecting most signal events. This is sufficient to carry out the calibration of the pmts. However, if we want to identify the physical threshold and want to obtain a plot of the spectra given in physical units, instead of attenuation unit, we can use a simple model to convert attenuation values to mV:

$$f(att) = \frac{a}{(x - b)^c + d}$$

Specifical values of  $a, b, c, d$  are suggested in the NINO board documentation. So the spectra values in physical units are represented by:



### 4.3.6 Autocalibration procedure

In this section we present the last calibration techniques needed in the data-process. The autocalibration is a special operation mode of the MAMI accelerator, during which the beam current is made to vary in a controlled way. Through these special runs it is possible to obtain again the current scaling factor that we discussed in 4.3.4. Because the current is varying, it is possible to study the linearity of the pmts. From a linear fit of the pmts counts vs. current intensity the angular coefficient and the offset are measured. The offset is particularly important because it gives rise of a possible systematic error that influences the final asymmetry result. It is quite simple to demonstrate this, if a relation of the type  $N = mI + N_0$  holds. Consider the following quantity:

$$\bar{N} = \frac{N_\uparrow + N_\downarrow}{2}$$

we can express  $N_\uparrow$  and  $N_\downarrow$  in this way:

$$N_\uparrow = \bar{N} + A_n \bar{N}$$

$$N_\downarrow = \bar{N} - A_n \bar{N}$$

Now we suppose that  $\bar{N}$  is linear dependent on the current in the way we defined above, so:

$$N_\uparrow = \bar{N} + A_n(mI) + N_0$$

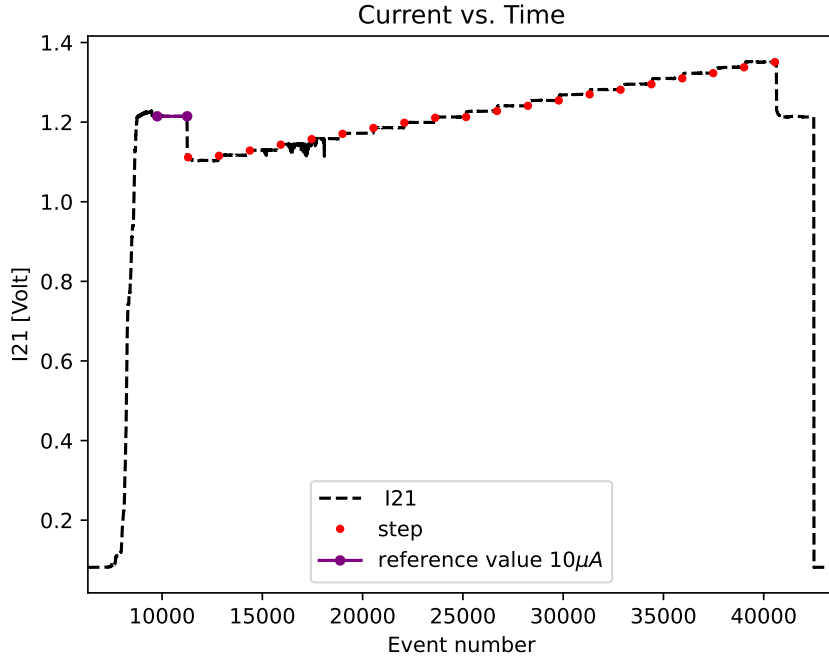
$$N_\downarrow = \bar{N} - A_n(mI) + N_0$$

We are supposing that the offset  $N_0$ , we assume that the present offset does not contribute to the asymmetry, i.e. it is not correlated to the signal of the scattered electrons, but is due to processes of another type, therefore in the previous formulas only the  $mI$  counts must be multiplied by the asymmetry  $A_n$ . Therefore if we substitute everything in the definition of the transverse asymmetry:

$$A' = \frac{N_\uparrow - N_\downarrow}{N_\uparrow + N_\downarrow} = \frac{A_n(2mI)}{(2mI) + 2N_0} = A_n \frac{1}{1 + \frac{N_0}{mI}} \quad (4.6)$$

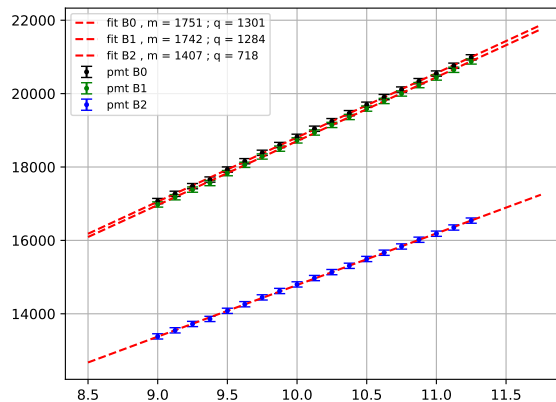
In the last passage we learn that the presence of an offset can decrease the reconstructed asymmetry. So it's important to determine quantitatively  $N_0$  and  $m$  in order to be able to take care of this effect. The strategy used is quite simple: every three hours of production data, we asked MAMI to start the autocalibration program. With all the autocalibration runs, we estimate  $N_0$  for each pmt, separately. Then all this quantities are saved in a file so that the analysis program can retrieve the parameters and subtract them from the pmt counts. In this way every three hours the pmts are corrected, this takes care also of the possibility that the linearity of the pmts can change after hours of use of the pmts (for example it can decrease the efficiency).

During the autocalibration, the beam current is raised from 9  $\mu\text{A}$  to 11,125  $\mu\text{A}$  in step of 0,125  $\mu\text{A}$ :

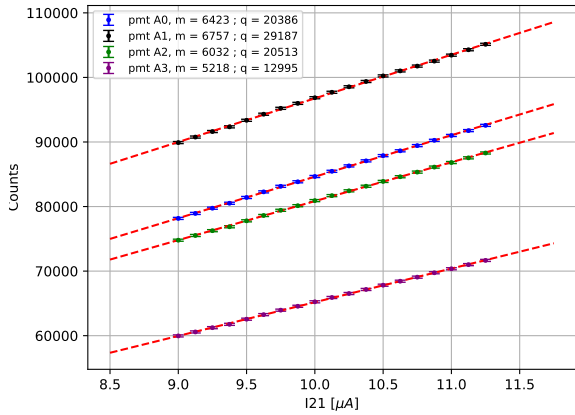


(a) Autocalibration: in this plot we have the voltage value of I21 monitor. The current is first stabilized around  $10\text{ }\mu\text{A}$ , then it is raised from  $9\text{ }\mu\text{A}$  (the step lower down) to  $11,125\text{ }\mu\text{A}$  in step of  $0,125\text{ }\mu\text{A}$ .

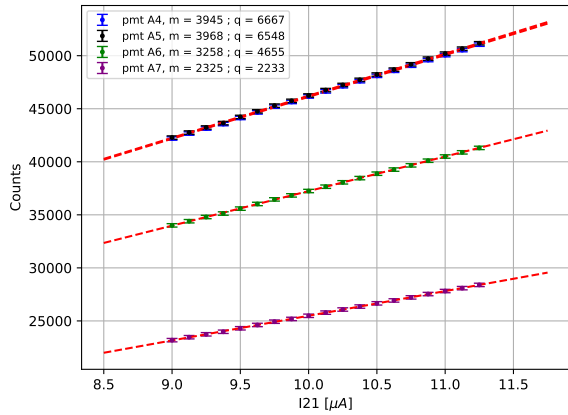
With a linear fit we can estimate the scale and the offset to convert from I21 voltage values to physical values of the current. The procedure is repeated for the 8 autocalibration acquisition we had during the beam time, so we can also take care of possible variations during the time.



(a) Current scan for detector B, the error are multiplied by a factor of 20.



(a) Current scan for detector A, the error are multiplied by a factor of 20.



(b) Current scan for detector A, the error are multiplied by a factor of 20.

Figure 4.11: Pmt Rates vs current (from I21 monitor), the model used for the fit:  $y = mx + q$ .

The figures are referred to the data acquired for the first autocalibration. It's interesting to calculate, from the result of the fit, the factor that appears in 4.6:

PMT	$m$ [ $\mu\text{A}^{-1}$ ]	Offset	c
B0	1750	1301	0.93
B1	1742	1283	0.93
B2	1406	717	0.95
A0	6423	20385	0.75
A1	6756	29187	0.70
A2	6032	20513	0.75
A3	5218	12995	0.80
A4	3945	6666	0.86
A5	3967	6547	0.86
A6	3258	4655	0.87
A7	2325	2233	0.91

Ignoring the presence of the offset lead two consequences: the reconstructed asymmetry is lower, on average  $\simeq 10\%$  less than expected, and the Counts are overestimated. Because the error depend on the pmt counts, as seen in 2.7, this two effect combined add up and worsen the precision and accuracy of the measurement. The result reported in the table can be confronted with the final result that are reported in 6.

# Chapter 5

## Data Analysis: Asymmetry on Carbon and Rates on Lead target.

### 5.1 Rates on lead

This section is straightforward. Basically I have to show the single plot of the pmts counts vs. beam current for lead target. However it's possible to do some preliminary studies, for example to calculate the time needed for measuring the asymmetry on lead with a certain error and maybe check from Mott cross section that the observed rate are fine.

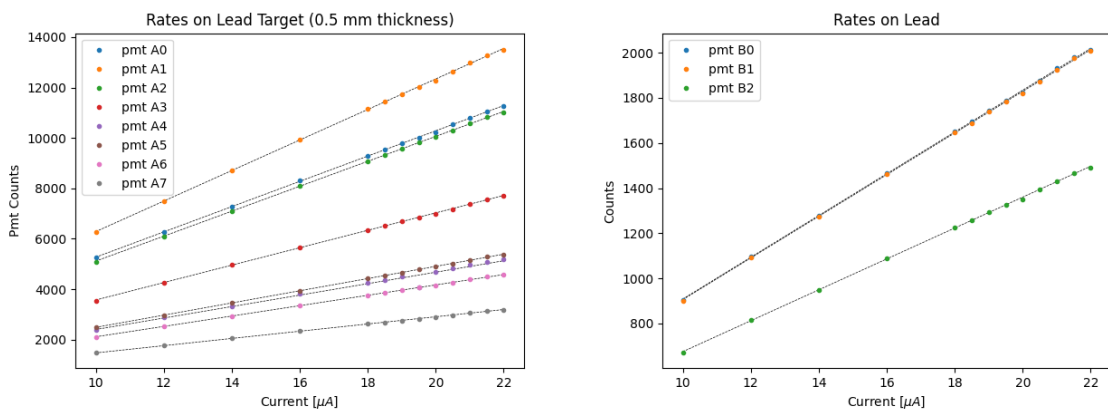


Figure 5.1: Rates on lead Target, for Detector A (left)

### 5.2 Model for fitting the data

Here I have to explain the model used for describing the data, so the problem of the false asymmetry induced by variations in beam position, angle, current and energy.

One of the problems of the measurement is to take into consideration the various contributions that can change the value of the asymmetry measured by the experimental apparatus. The raw values of the asymmetry can be affected by the variation of the beam parameters during the time. Let's summarize quickly all these effects:

- the pmts counts can depend on the  $(x, y)$  impact position of the beam on the target
- the variations of the incident angles  $\theta_x$  and  $\theta_y$  on the target.
- the uncertain associated with the energy of the Beam, a change in the energy associated with the polarization of the beam leads to different rates for the cross section
- the uncertain associated with the current of the Beam, in particular a change due to the efficiency of the source in producing electrons polarized in the two opposite directions

All this quantity can influence the asymmetry measured by the pmts, considering also that the expected asymmetry is in the order of ten part per million, and small asymmetry introduced by fluctuations on the beam parameters are not negligible. Correcting directly the false asymmetries that rise from those uncertainties is a tough task, and it's more easy to adopt a different strategy respect to proceed to the analytical/numerical calculation of each of them . Knowing that the beam parameters produced by Mami are quite stable over the time, we can assume that the measured asymmetry are well described by a linear model as the following:

$$Asym = A_{physical} \cdot P + \delta_I + A_x \delta x + A_y \delta y + A_{\theta_x} \delta \theta_x + A_{\theta_y} \delta \theta_y + A_E \delta E \quad (5.1)$$

$A_{physical}$  is the aim of the experiment,  $A_x$  and  $A_y$  are the asymmetries induced by the variation of the position of the beam,  $A_{\theta_x}$  and  $A_{\theta_y}$  are the asymmetry associated to angles,  $A_E$  is the asymmetry associated to the beam energy. The relevant assumption is that, for small variation of the beam, the false asymmetry are linearly dependent on the Beam uncertainties (that are  $\delta x, \delta y, \delta \theta_x, \delta \theta_y, delta_E$ ), so a first order approximation seems valid.

We must clarify now what we mean with  $\delta x, \delta y, \delta \theta_x, \delta \theta_y, delta_E$ . Resuming the event structure, that we discussed in 3.1, we have a sequence of 4 different sub-events, with a polarization pattern that is randomly selected between  $\uparrow, \downarrow, \downarrow, \uparrow$  and  $\downarrow, \uparrow, \uparrow, \downarrow$ . During the 20 ms ot time lenght of each sub-event, the vfcs make a single measurement of the beam, and the data are saved in the data tree. The task of the analysis program is to use this raw data to calculate the relevant parameters for the analysis. Because we are working with asymmetries, the absolute values of the parameters listed above is not relevant, instead what is relevant are the differencies correlated with polarization state of the beam. Assuming this,  $\delta x, \delta y, \delta \theta_x, \delta \theta_y, delta_E$  are replaced with :

$$\begin{aligned} \delta x &= \left( \frac{X_{\uparrow}(1) + X_{\uparrow}(2)}{2} \right) - \left( \frac{X_{\downarrow}(1) + X_{\downarrow}(2)}{2} \right) \\ \delta y &= \left( \frac{Y_{\uparrow}(1) + Y_{\uparrow}(2)}{2} \right) - \left( \frac{Y_{\downarrow}(1) + Y_{\downarrow}(2)}{2} \right) \\ \delta E &= \left( \frac{E_{\uparrow}(1) + E_{\uparrow}(2)}{2} \right) - \left( \frac{E_{\downarrow}(1) + E_{\downarrow}(2)}{2} \right) \\ \delta \theta_x &= \left( \frac{\theta_{x,\uparrow}(1) + \theta_{x,\uparrow}(2)}{2} \right) - \left( \frac{\theta_{x,\downarrow}(1) + \theta_{x,\downarrow}(2)}{2} \right) \\ \delta \theta_y &= \left( \frac{\theta_{y,\uparrow}(1) + \theta_{y,\uparrow}(2)}{2} \right) - \left( \frac{\theta_{y,\downarrow}(1) + \theta_{y,\downarrow}(2)}{2} \right) \end{aligned} \quad (5.2)$$

Each value represent the difference between the mean values over the two different polarization state.

### 5.3 Data pre-selection and Fit

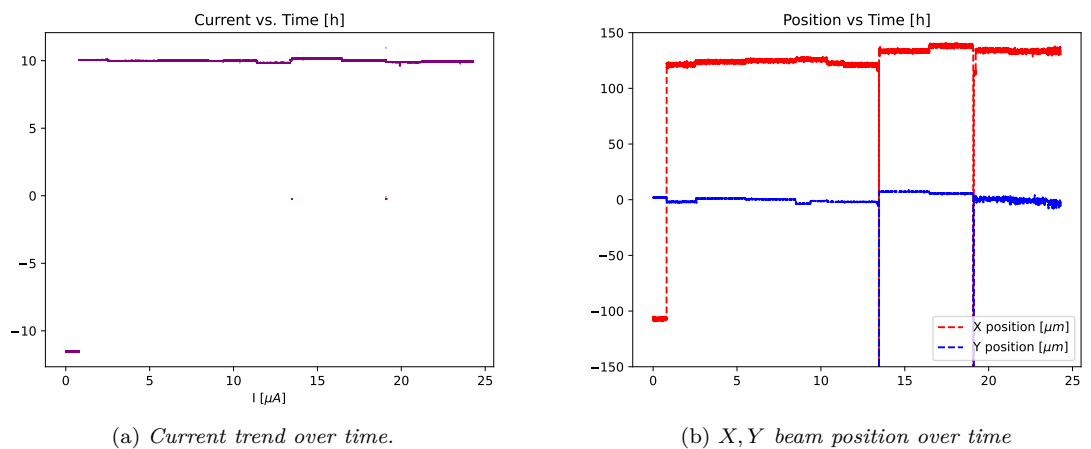
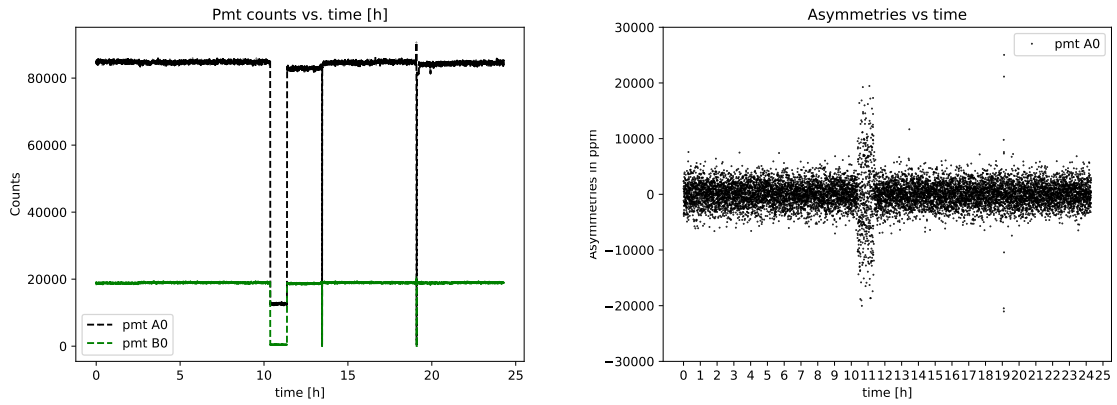
After all the calibration are performed, the analysis program is ready to produce the datafiles suitable to analyze the asymmetry data for Carbon.

The Data file that are produced from the binary files are simply files in txt format, where the data are stored in columns. Before proceeding with the linear fit, however, it is necessary to visualize the data to check that there are no anomalous behaviors. In fact the data can contain moments of loss of the beam burrent and sudden interruptions, loss of polarization of the beam and even setting errors by MAMI operators can affect the experiment. Carbon data were taken from November 2nd to 4th, and consist of 28 runs, each 1 hour long. The first step is to observe the pmt counts and the current trend, in order to be able to identify sudden interruptions of the beam. Here we show the trend over time for the series runs:

This plot show that after 10 h of data acquisition the Pmt counts (5.2a) dropped rapidly. If we show the current trend over the time (5.2a) we do not see a corresponding decrease in beam intensity. Also the  $x, y$  position (5.2b) and the energy monitor of the beam do not show a strange behavior. So we reject the possibility that at some point one of the stabilization device of the beam stop working. One of the possibilities is that something happen inside the two spectrometers. From the pmt counts we can suggest that the scattered electrons were not hitting our fused-silica detector, in fact for pmt B0 we observe roughly 0 counts, and for pmt A0 20000 counts, which is compatible with the noisy offset of that pmt. This consideration strongly suggest as to reject those data from the analysis.

Apart from this, we observe in (4) two steepy variations of the asymmetry around 13.5h and 19h. For these data is quite simple to explain why should be rejected: we observe the same steepy variations also for the positions, so in this case the beam was not correctly aligned to the target.

After this first data selection, we check the correlated-difference data, which will be later used as variables for the fit. We produced histograms for all this quantites, that we remember are computed by the analysis program with the formula:

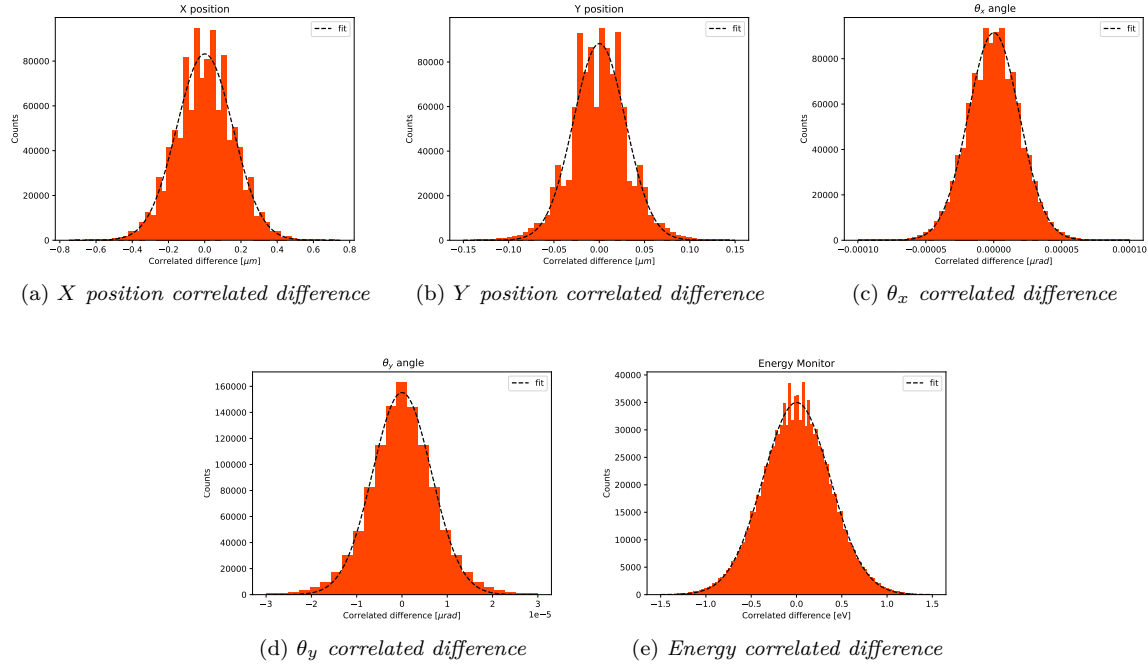


$$\delta x = \frac{(x_{up,1} + x_{up,2})}{2} - \frac{(x_{down,1} + x_{down,2})}{2}$$

We expect, if the stabilization of the beam is correctly set, that those quantities are gaussian distributed. A maximum likelihood fit with a Gaussian model is performed for each beam parameter, with Likelihood Ratio for the goodness of fit (gof). The statistic for the gof is:

$$\lambda(x) = 2 \sum_i^n (f_i(\mu) - k_i(1 + \log(\frac{f_i(\mu)}{k_i})))$$

$\mu$  are the parameters of the *pdf*, that are mean and variance of the gaussian, and  $f_i(\mu)$  and  $k_i$  are respectively the expected value for the i-nth bin and the observed value for the i-nth bin.



Looking at the histograms, we see that the beam correlated-difference values are centered around zero, the result are reported below:

	$X[\mu\text{m}]$	$Y[\mu\text{m}]$	$Xp[\mu\text{rad}]$	$Yp[\mu\text{rad}]$	$E[\text{eV}]$
$\mu$	$1.31 \cdot 10^{-3}$	$2.4 \cdot 10^{-4}$	$3.2 \cdot 10^{-8}$	$3.6 \cdot 10^{-9}$	0.0013
$\sigma$	$3.7 \cdot 10^{-1}$	$2.9 \cdot 10^{-2}$	$1.9 \cdot 10^{-5}$	$6.5 \cdot 10^{-6}$	0.38

these results are encouraging, the stabilization of the beam has meant that only small differences are observed within an event for each monitor. This means that, unless the values for the false asymmetries are not very large, the effect of the beam variation are small. Before proceeding with the fit, we observe how the asymmetry evolves as a function of time.

In this figure we plot the average of the asymmetries for each pmt, carried out from the beginning up to the instant  $t$ . The data shown are corrected with the percentage of polarization of the beam ( $p \simeq 0.79$ ). From this it can be seen how the asymmetry evolves as time increases. If there are still outliers data, we can directly check from this plot there a steepy variation in the data.

When all the calibrations are performed, it is possible to proceed to generate the datafiles for the fit program.

For a better visualization of the data, especially to observe the dependence of the asymmetry on the Beam parameters measured, it is useful to take the average asymmetry at regular intervals. From the raw plots of the asymmetries (see below 5.3), it is clear that the statistical error associated to the asymmetry is the main one, and it's not possible to identify a linear dependence. In the meantime, this plot shows that there is a difference in sign between the values measured by the two detectors, and that at the end the averaged result are on the same order of magnitude of what we expect  $\pm 20$  ppm at our scattering angle  $\theta$ . These results, coupled with the fact that the correlated differences in beam values are small, suggest that the contribution of false asymmetries is limited.

In some plots (X,Y and I) we can identify equally spaced cluster of data. So we decide to compute the averaged asymmetry for each cluster we were able to identify. In the following plots we decided to apply some cuts to the data, selecting only the events where the values of all the monitor are less than 3 standard deviation far from the mean. In all the figures the asymmetries are multiplied by a factor of  $10^6$  to have the result in ppm (so each y-axis is in ppm).

$$(x_{\text{monitor}} - \bar{x}_{\text{monitor}}) \leq 3 \cdot \sigma_X$$

For each monitor we use the *curve fit* function of the python library `scipy` to fit the data. Each Beam parameter is treated separately now, so in principle we are ignoring possible effect of correlation between the X-values (however, from the correlation matrix *write that somewhere* the effects are negligible)

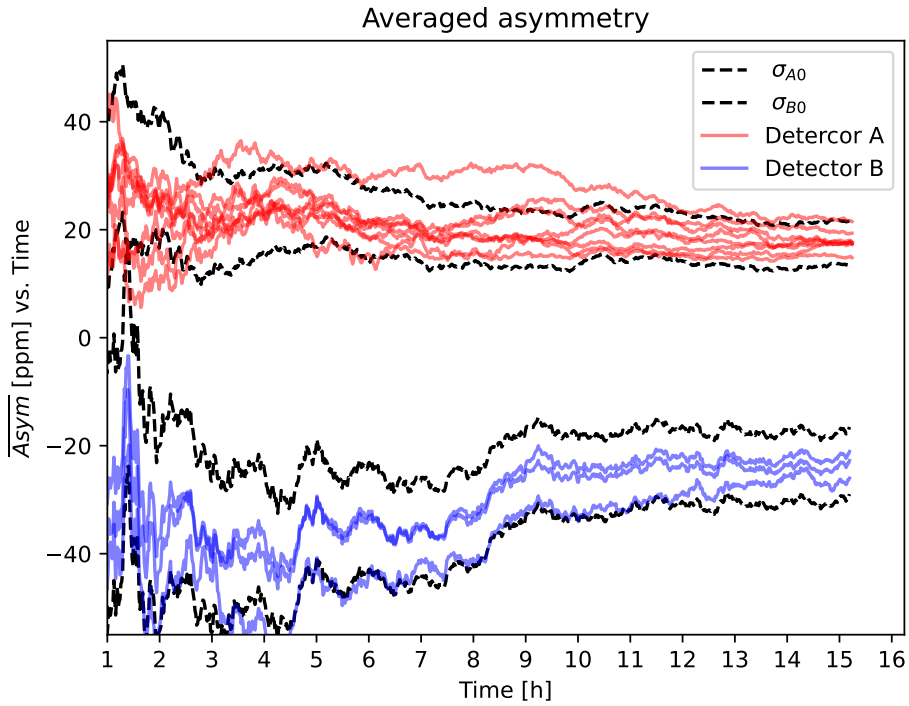


Figure 5.2: Plot of the Asymmetry versus time. For a point time  $t_1$ , we plot the mean over all the asymmetries collected from  $t = 0$  to  $t = t_1$ . Each line represents the asymmetries measured for a specific pmt (in blue detector B and in red detector A). The values are corrected for the beam polarization, multiplying by  $\frac{1}{p}$ . We plot also the error, which is one standard deviation  $\sigma$  from the mean.

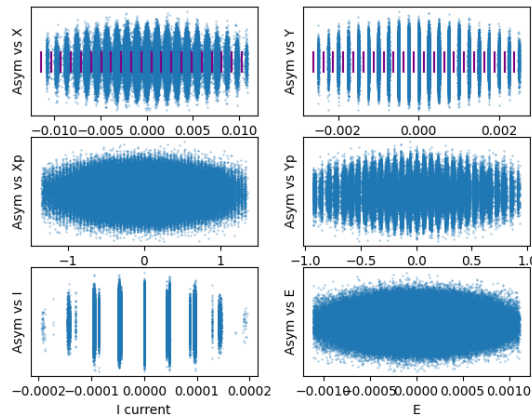
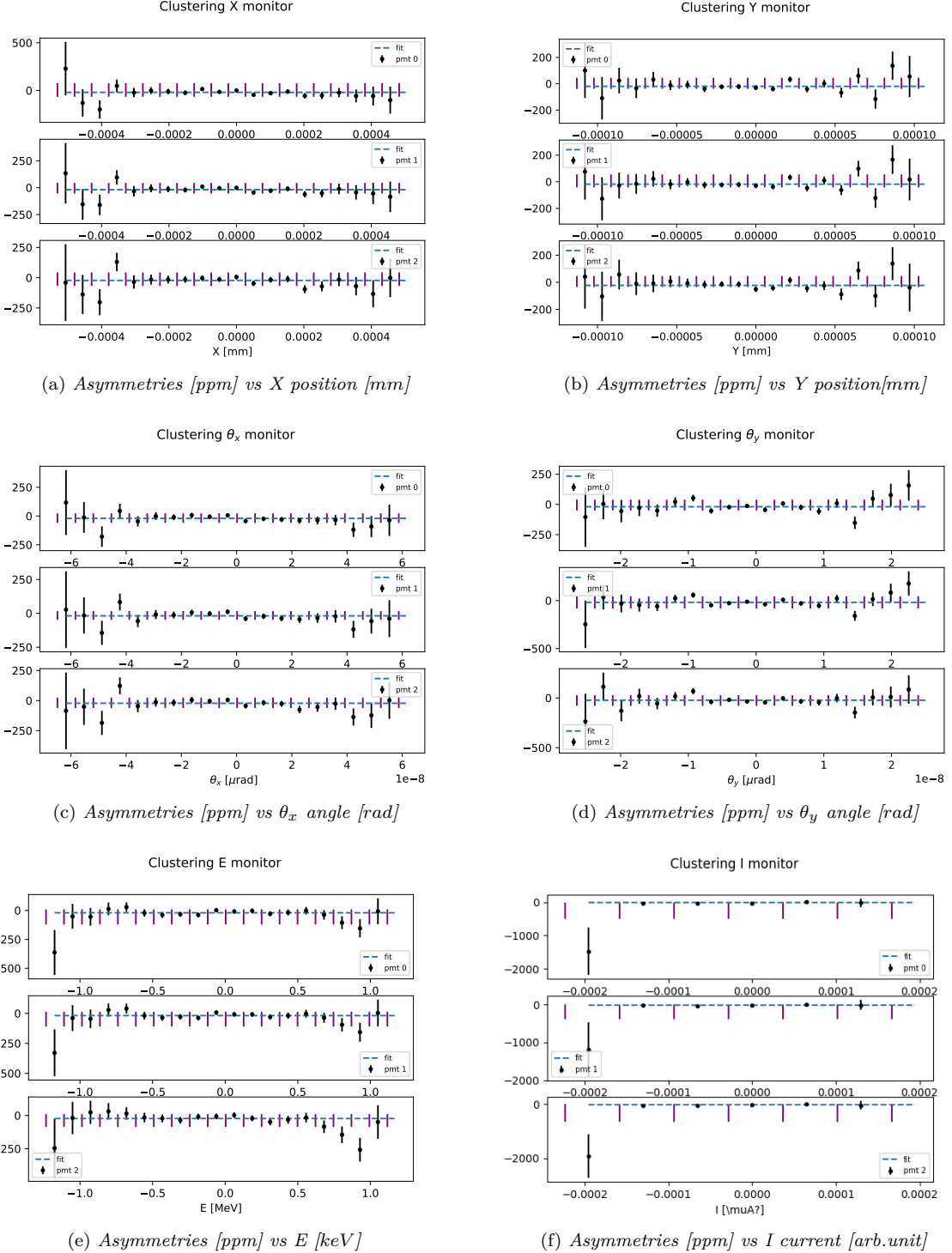


Figure 5.3: Asymmetries vs. Beam parameters



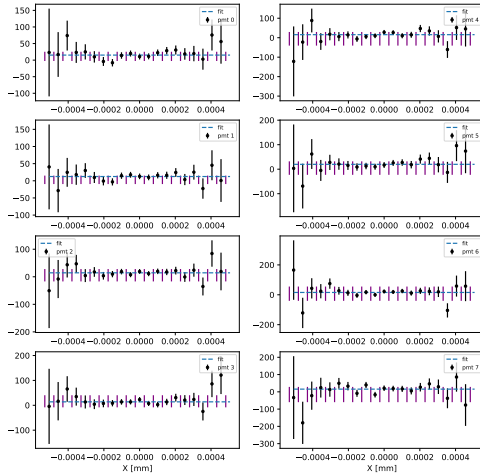
The error of each point is computed exploiting the same formula defined above (theory section;  $N_{A/B}$  averaged pmt counts for each subevents and  $n$  number of event in each interval):

$$\sigma_{Asym} = \frac{1}{\sqrt{2N_{A/B} \cdot n}}$$

## 5.4 False asymmetries

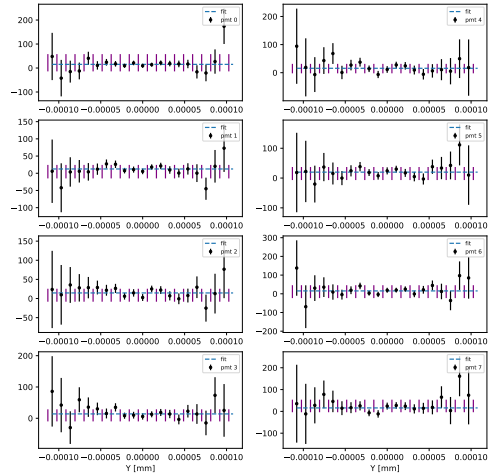
Seems that is possible to obtain rough estimates of the beam related asymmetries with the results from the fit. For Energy and position it's achievable, while for the angles it's quite hard (in principle sounds possible to perform an analytic calculation of the asymmetry related to the incident beam angle, however Anselm told me that quite often those results are in disagreement with the observed even in the sign!).

Clustering X monitor



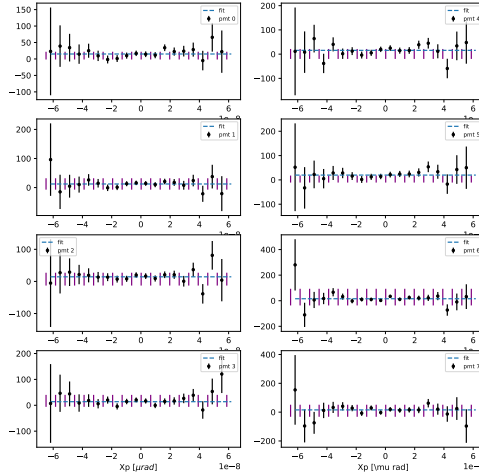
(a) Asymmetries [ppm] vs X position [mm]

Clustering Y monitor



(b) Asymmetries [ppm] vs Y position [mm]

Clustering Xp monitor

(c) Asymmetries [ppm] vs  $\theta_x$  angle [rad]

Until now the values for the false asymmetries were treated as the parameters of the fit. In this section we will investigate how we can obtain another different estimations, useful to check the validity of all the process of analysis of the data.

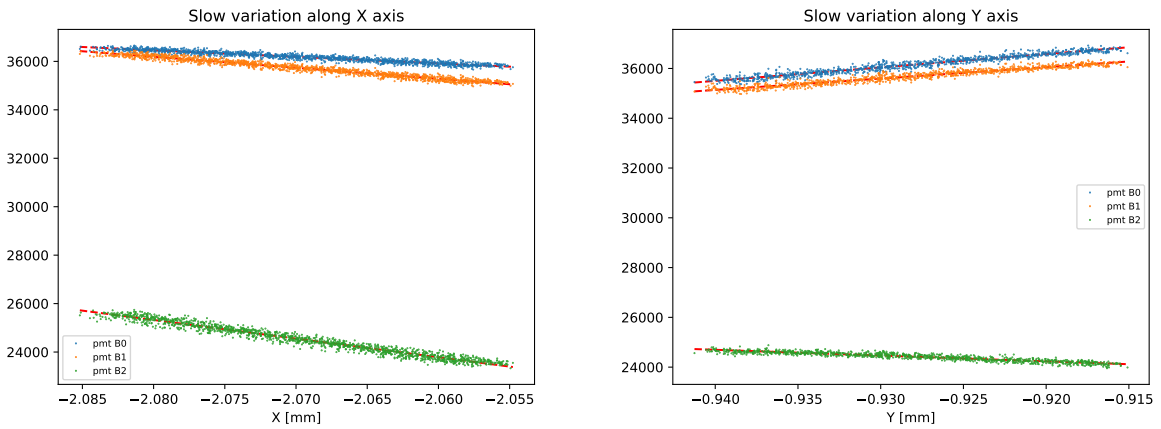
For  $\frac{dA}{dX}$  and  $\frac{dA}{dY}$ , we conceptually exploit the possibility of varying the position of the beam on the target, as we did during one of the calibration phases. Using the same *wobbler 16* we asked MAMI to slowly change the beam position on the X and Y monitor. The change in position has the effect to modify the rates for the two detector, and from them it's possible to extract estimate the two false asymmetries related to the beam position. Now we will see how the two quantities are related. From the plot .. we see that the counts are scaling linearly with the beam position, so we assume that the  $N$  are given by

$$N(x, \dots) = N_0 + m \cdot (x - x_0)$$

it is clear that the linear model can't be always good, at some point the electron will be deflected completely out of the detector, and so the counts will fall rapidly to zero. However, the magnets used to deflect the beam are producing small variation in the position, on the order of hundredths of a millimeters. Let's suppose that the beam position for two sub-events is  $x_1$  and  $x_2$ , we can calculate the asymmetry between the two event, taking care of the possible effects due to the different position. We write explicitly:

$$Asym = \frac{N(x_1) - N(x_2)}{N(x_1) + N(x_2)} = \frac{N_0 + m \cdot (x_1 - x_0) - N_0 - m \cdot (x_2 - x_0)}{N(x_1) + N(x_2)} = \frac{m}{2N_0 + m \cdot (x_1 + x_2) - 2mx_0} (x_1 - x_2) \quad (5.3)$$

In this equation three different parameters appear:  $N_0$  is the offset of the linear model,  $m$  is the angular coefficient, or the slope, and  $x_0$  is the initial position respect to we compute the position variation. The first two terms are obtained by a linear fit, while  $x_0$  is fixed conveniently.



We can approximate the denominator deleting the term  $m \cdot (x_1 + x_2)$  which should be small compared to  $2N_0$ . We end with:

$$Asym = \frac{m}{2N_0 - 2mx_0} (x_1 - x_2) \quad (5.4)$$

The term in front of  $(x_1 - x_2)$  can be compared to  $\frac{dA}{dX}$ .  $x_0$  is arbitrary and can be set to 0. For  $N_0$ , the offset, we substitute the averaged value counts of each pmt for the polarized beam acquisitions (we remind that the rate are collected during each 20 ms time interval of each sub-event).

The data are reported in the table below:

Pmt	Detector A	Detector B
pmt 0	84718	18925
pmt 1	96882	18815
pmt 2	80604	14807
pmt 3	65053	
pmt 4	45943	
pmt 5	46248	
pmt 6	37452	
pmt 7	25808	

We report the values obtained with this new method ...

We can investigate also the asymmetries related to the beam energy. For this one we can exploit the theoretical expression for the Mott cross-section, taking the derivative ...

We can investigate the Current asymmetries, because we have the autocalibration procedure, so from the scale factor we can check if the current asymmetri is compatible with 1 as assumed or not.

## 5.5 ??Bootstrap??

Although Anselm was against it, now seems possible to increase the precision of the mesurement with a procedure similar to a bootstrap. Instead of computing all the quantities inside a single event, it's possible to compute all the important quantities also between different events. In this scenario the statistics can be increased artificially as mutch as we want, with the same amount of data. Of course, it's also simple to abuse of this method, so we should restrict using only events next to each other. However seem reasonable and promising.

# Chapter 6

## Result

- asymmetries on carbon.
- expected rates on lead.
- false asymmetries result.
- average of the asymmetries for the pmts.
- confront with the theory.

In this chapter we report the result obtained for the data-analysis. First we report the averaged asymmetries with and without subtracting the pmt offset. From the asymmetry results, we can compute the factor  $c$  as the ratio between the final asymmetries with and without subtracting the offset. The values can be directly confronted with the ones defined in 4.3.6. We see a good agreement. All the values are in ppm (part-per-million).

PMT	Average	$\sigma$	PMT	Average	$\sigma$	PMT	$c$
B0	-21.64	7.9	B0	-22.46	7.9	B0	0.96
B1	-19.96	7.9	B1	-20.73	7.9	B1	0.96
B2	-24.91	8.9	B2	-25.33	8.9	B2	0.98
A0	18.83	3.7	A0	24.25	3.7	A0	0.78
A1	15.92	3.5	A1	21.6	3.5	A1	0.74
A2	18.8	3.8	A2	24.25	3.8	A2	0.78
A3	18.54	4.2	A3	22.58	4.2	A3	0.82
A4	20.47	5	A4	23.53	5	A4	0.87
A5	22.61	5	A5	25.88	5	A5	0.87
A6	18.45	5.6	A6	20.86	5.6	A6	0.88
A7	18.41	6.7	A7	19.89	6.7	A7	0.93

(a) Asymmetries, with offset not subtracted.  
(b) Asymmetries with offsets subtracted.  
(c)  $c$  factor, as defined in 4.6

Table 6.1: Averaged asymmetries over all the events. The values are corrected subtracting  $\bar{A}_I$  and considering the effective polarization  $p$  of the beam

The asymmetries are shown with the errors in the following plot. The error are obtained with the formula:

$$\sigma = \sqrt{\frac{1}{2N \cdot n}}$$

To Obtain a final asymmetry for detector A and B, the asymmetries for each plot are averaged using the formula:

$$\bar{A}_n = \sum_{i=0}^{n_{PMT}} \frac{w_i A_i}{\sum_{i=0}^{n_{PMT}} w_i} \quad (6.1)$$

This is a weighted mean, and  $w_i = \frac{1}{\sigma_i^2}$ . This formula is applied to take care of the different statistical error for different pmts.

The final result obtained, without any further analysis, are:

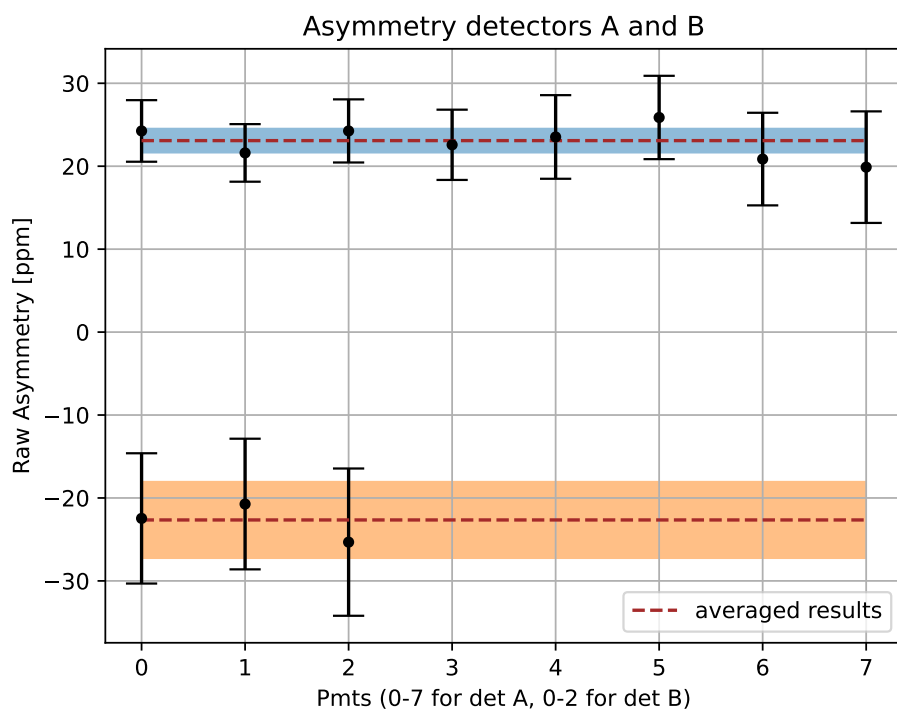


Figure 6.1: Plot of the asymmetries ordered by the pmt label, the result are the average event per event, corrected by the beam asymmetry current and for the polarization  $p$  percentage.

- Asymmetry for detector A,  $A_A = 23.1 \pm 1.6$  ppm.
- Asymmetry for detector B,  $A_B = -22.7 \pm 4.7$  ppm.

## Chapter 7

# Conclusion and outlook

- outlook for the future experiments with lead.
- mention the future experiment with Parity-violatin scattering.

# Appendices

## **Appendix A**

### **Some Appendix**

The contents...

# Bibliography

- [1] Single and multichannel, synchronous voltage-to-frequency converters, ad7741. *Analog Devices*.
- [2] Strahldiagnostik und analyse der optischen eigenschaften des strahlführungssystems von mami. *Diplomarbeit*, 2004.
- [3] A. Esser, M. Thiel, P. Achenbach, K. Aulenbacher, S. Baunack, J. Beričić, D. Bosnar, L. Correa, M. Dehn, M. O. Distler, H. Fonvieille, I. Friščić, M. Gorchtein, S. Heidrich, P. Herrmann, M. Hoek, S. Kegel, Y. Kohl, T. Kolar, H.-J. Kreidel, F. E. Maas, H. Merkel, M. Mihovilović, J. Müller, U. Müller, F. Nillius, C. Palatchi, K. D. Paschke, J. Pochodzalla, B. S. Schlimme, M. Schoth, F. Schulz, S. Širca, B. Spruck, S. Štajner, V. Tioukine, A. Tyukin, A. Weber, and C. Sfienti. First measurement of the  $Q^2$  dependence of the beam-normal single spin asymmetry for elastic scattering off carbon. *Phys. Rev. Lett.*, 121:022503, Jul 2018.
- [4] M. Gorchtein and C. J. Horowitz. Analyzing power in elastic scattering of electrons off a spin-0 target. *Physical Review C*, 77(4), apr 2008.
- [5] B.S. Schlimme, P. Achenbach, K. Aulenbacher, S. Baunack, D. Bender, J. Beričić, D. Bosnar, L. Correa, M. Dehn, M.O. Distler, A. Esser, H. Fonvieille, I. Friščić, B. Gutheil, P. Herrmann, M. Hoek, S. Kegel, Y. Kohl, T. Kolar, H.-J. Kreidel, F. Maas, H. Merkel, M. Mihovilović, J. Müller, U. Müller, F. Nillius, A. Nuck, J. Pochodzalla, M. Schoth, F. Schulz, C. Sfienti, S. Širca, B. Spruck, S. Štajner, M. Thiel, V. Tioukine, A. Tyukin, and A. Weber. Vertical beam polarization at MAMI. *Nuclear Instruments and Methods in Physics Research Section A: Accelerators, Spectrometers, Detectors and Associated Equipment*, 850:54–60, apr 2017.